Preprint submitted to Remote Sensing of Environment April 02nd, 2022

Monitoring shifting cultivation in Laos by combining time series analysis and object-based analysis

Shijuan Chen* (shijuan@bu.edu) (1)

Pontus Olofsson (olofsson@bu.edu) (1)

Thatheva Saphangthong (thatheva@gmail.com) (2)

Curtis E. Woodcock (curtis@bu.edu) (1)

1. Department of Earth and Environment, Boston University, 685 Commonwealth Avenue, Boston, MA 02215, United States

2. Department of Agriculture Land Management, Ministry of Agriculture and Forestry, Lao PDR

* Corresponding author: Tel.: +1-(617)-358-0503

Keywords: Disturbance; Forest degradation; Deforestation; Shifting cultivation; Shifting agriculture; Slash and burn; Swidden agriculture; Landsat; Google Earth Engine; Time series analysis; CCDC-SMA; Object-based image analysis.

Highlights:

1. Time series analysis and OBIA are combined to attribute forest disturbance.
2. Shifting cultivation, new plantation, and deforestation are mapped in Laos.
3. Shifting cultivation is mapped with high accuracy (producer's: 88%; user's: 80%).
4. Shifting cultivation affected 32.9% ± 1.9% of Laos from 1991 to 2020.
5. Slash-and-burn activities in Laos increased in the most recent 5 years.

Abstract

Shifting cultivation is an important driver of forest disturbance in the tropics. However, studies of shifting cultivation are limited and current area estimates of shifting cultivation are highly uncertain. Although Southeast Asia is a hotspot of shifting cultivation, there are no national maps of shifting cultivation in Southeast Asia at moderate or high resolution (less than or equal to 30 m). Monitoring shifting cultivation is challenging because the slash-and-burn events are highly dynamic and small in size. In this research, we present and test an approach to monitoring shifting cultivation using Landsat data on Google Earth Engine. CCDC-SMA (Continuous Change Detection and Classification - Spectral Mixture Analysis) is used to detect forest disturbances. Then, these disturbances are attributed by combining time series analysis, object-based image analysis (OBIA), and post-disturbance land-cover classification. Forest disturbances are assigned to *Shifting cultivation*, *New plantation*, *Deforestation*, *Severe drought*, and *Subtle disturbance* annually from 1991 to 2020 at a 30-meter resolution for the country of Laos. The major forest disturbances in 1991-2020 are mapped with an overall accuracy of 85%.

Shifting cultivation is mapped with a producer's accuracy of 88% and a user's accuracy of 80%. The margin of error of the sampling-based area estimate of *Shifting cultivation* is 5.9%. The area estimates indicate that shifting cultivation is the main type of forest-disturbance in Laos, affecting 32.9% ± 1.9% of Laos over the past 30 years. To study the development of shifting cultivation over time, the area of slash-and-burn events is estimated at 5-year intervals of 1991-2020 with all margins of error less than 17%. Results show that the area of slash-and-burn activities in Laos increased in the most recent 5-year period. We believe that the methods developed and tested in Laos can be applied to other regions.

1 Introduction

Shifting cultivation, also called “shifting agriculture”, “swidden agriculture”, or “slash and burn”, is a farming practice where farmers clear and burn the native forest to create an ash-fertilized soil. Crops are then planted and harvested for one or two years in succession, after which the plot is abandoned, and the practice repeated in an adjacent patch of forest. If the cultivated plot is left fallow for long enough before being cultivated again, the forest and soil can recover. As such, rather infrequent rotations from forest to crop and back to forest were sustainable for generations, but with increased population pressure, farmers often cultivate the land before the vegetation and soil have recovered (Hillel, 2007). The result is a complex landscape composed of patches of cleared land, fallow land and forests of different ages, species composition, and, crucially, reduced carbon stocks (Villa et al., 2021).

Shifting cultivation is one of the major drivers of forest degradation in the tropics (Curtis et al., 2018). Here we treat shifting cultivation as a form of forest degradation because the land cover is mostly forest except for a short amount of time but with less biomass. The issue is complicated though; the current REDD+ (Reducing Emissions from Deforestation and forest Degradation) reporting practices do not address the issue of shifting cultivation as most definitions of forest used in REDD+ reporting are based on the percentage of canopy cover in a given spatial unit. These definitions are inadequate to represent the mosaic landscapes of cyclic shifts between forest and non-forest as a result of shifting cultivation. The phenomenon of temporary and cyclic change in land use was mentioned by the IPCC, who attempted to resolve the definition of degradation, but no resolution was achieved as temporary changes are not necessarily unsustainable, even if the carbon stock is reduced (Herold & Skutsch, 2011). The Global Forest Observation Initiative of the Group on Earth Observations (GEO-GFOI) has released three versions of a Methods & Guidance Document that aims to put the IPCC guidelines for reporting under REDD+ in a practical context. The Methods & Guidance Document states that (GFOI, 2020, p. 78)

> *"In countries where there are multiple clearing and regrowth cycles (shifting agriculture being an example) it will be necessary to not only estimate emissions from the initial clearing, but also to estimate the removal and subsequent future emissions during repeated cycles of clearing and regrowth. This can be done by either tracking the changes through time or by developing a manageable number of statistically representative strata to represent these land uses."*

and further that (GFOI, 2020, p. 96)

> *"There is wide agreement that forest degradation represents long-term loss of forest values, and that temporary loss due to harvest or natural disturbance in sustainably managed forest is not degradation."*

Economic demand and population pressure have forced the practice of shifting cultivation away from sustainably long rotations to more frequent cultivation that does not allow the vegetation and soil to rejuvenate (Hillel, 2007). Such developments weaken the argument that shifting cultivation qualifies as sustainable forest management. Hence, shifting cultivation should be considered forest degradation in the REDD+ context.

Shifting cultivation is understudied although it has been identified as an important driver of forest degradation (Curtis et al., 2018) and has long-term carbon impacts (Ziegler et al., 2012). Three global maps of shifting cultivation have been produced in the previous studies. The first one is a hand-drawn map of global shifting cultivation created by Butler (1980) showing the distribution of shifting cultivation. The second is a one-degree resolution map made by Heinimann et al. (2017) based on visual interpretation of the Global Forest Change (GFC) dataset (Hansen et al., 2013). The third map is a product of the 10-km resolution map of drivers of global forest disturbance created by Curtis et al. (2018) . The three maps represent the global distribution of shifting cultivation, but the resolutions (>10 km) are much larger than the scale of individual slash and burn events, which makes the maps hard to use for subsequent analyses including spatial-temporal patterns and carbon emissions of shifting cultivation. Studies of shifting cultivation at a national or regional level are limited and inconsistent in their reporting of trends (increasing, decreasing, and stable trajectories) (Van Vliet et al., 2012; Li et al., 2014). Southeast Asia is a hotspot of shifting cultivation, but previous studies of shifting cultivation in Southeast Asia have been mostly local (Messerli et al., 2009; Hett et al., 2012; Liao et al., 2015; Hurni et al., 2013a). There are several studies of land cover and land use change in Southeast Asia (e.g. Tang et al., 2021;Saah et al., 2020; Potapov et al., 2019; Langner et al., 2018), but without an explicit focus on forest degradation and shifting cultivation. To the authors' knowledge, no maps of shifting cultivation at moderate or high spatial resolutions (less than or equal to 30 m) exist in Southeast Asia at a national level.

Monitoring shifting cultivation is challenging since the slash-and-burn events are highly dynamic and fine-scale disturbances (Miettinen et al., 2014). A traditional approach to mapping shifting cultivation uses a single-year land cover map to create landscape mosaics consisting of forest and agriculture and detect shifting cultivation based on the spatial patterns (Messerli et al., 2009; Hett et al., 2012; Hurni et al., 2013a; Silva et al., 2011). The limitation of this approach is that the spatial resolution of the shifting cultivation map is coarse and depends on the size of the mosaics (usually several kilometers), and it cannot represent the temporal patterns of shifting cultivation. Another approach is classifying land cover at the pixel-level using multi-temporal images to map shifting cultivation (Adhikary et al., 2019; Kurien et al., 2019; Leisz and Rasmussen, 2012; Molinario et al., 2015; Department of Forestry, 2018). In this approach, the time interval of the land cover maps is essential, as the forest recovers quickly after the slash-and-burn activity. If the time interval is too long, the shifting cultivation regions might be misclassified as stable forests. As stated in GFOI (2020), it is necessary to identify the cycles of clearing and regrowth to properly track the emissions and removals associated with shifting cultivation, which is not a trivial task. Tracking rapid cycles of clearing and growth is nearly impossible with traditional approaches to change detection where only a couple of images acquired over the same area are compared. A more feasible approach is to use dense time series to monitor rapid landscape changes and characterize the growth after the disturbance (Woodcock et al., 2020).

The recent advancements of remote sensing, such as the open data policy (Woodcock et al., 2008), cloud computing platform (Gorelick et al., 2017), and time-series-based algorithms (Kennedy et al., 2010; Verbesselt et al., 2010; Zhu & Woodcock, 2014; Bullock et al., 2020; Chen et al., 2021) provide new opportunities for monitoring changes in highly dynamic landscapes. However, we have only found few studies that used time series analysis to monitor shifting cultivation locally: Dutrieux et al. (2016) and Jakovac et al. (2017) used Breaks For Additive Season and Trend (BFAST) to monitor shifting cultivation in a small region in Amazon; Das et al. (2021) used the time series of Normalized Difference Vegetation Index (NDVI) and Normalized Burn Ratio (NBR) (Miller and Thode, 2007) to detect shifting cultivation in several states in Northeast India; and Hurni et al. (2013b) used time series of MODIS data to monitor shifting cultivation in Northern Laos. Furthermore, there has been limited effort devoted to differentiating shifting cultivation from other disturbances. Because most case studies focus on a small region with intensive shifting cultivation, it is unclear whether these approaches work in a larger region with a mixture of shifting cultivation and other types of disturbances such as conversion of forests to plantations and deforestation. Müller et al. (2013) found that the active fire data (1-km resolution) from Moderate Resolution Imaging Spectroradiometer (MODIS) has potential to detect fires from shifting cultivation in Laos if the fire is larger than 1 km. Curtis et al. (2018) used decision trees based on the history of forest disturbance, population and fire data in 10×10 km grid cells to classify forest disturbance into shifting cultivation, forestry, wildfire, and deforestation. The limitation of these studies is that the minimum mapping unit is many times larger than the area of an individual slash-and-burn event. Finally, accuracy assessment of most cases studies of shifting cultivation that we found were either missing or incomplete (Li et al., 2018) and did not follow recommended practices of accuracy assessment and area estimation (Olofsson et al., 2013; Olofsson et al., 2014).

The objective of the research presented in this article was to develop and test an approach to monitoring shifting cultivation and apply it to Laos to estimate the area of shifting cultivation from 1991 to 2020. The approach was developed on Google Earth Engine (GEE) by combining time series analysis (Chen et al., 2021), object-based image analysis (OBIA), and post-disturbance land cover classification. We conducted accuracy assessment and area estimation of shifting cultivation in Laos following the practices outlined in Olofsson et al. (2014).

2 Study area

Our study area is the whole country of the Lao People's Democratic Republic (Lao PDR)) in Southeast Asia (**Fig. 1**). Laos has a tropical savanna climate dominated by the monsoons, with about 90% of the annual rain falling in the wet season from May to October (Cramb, R., 2020). The dry season occurs between November and April. Shifting cultivation is a significant land use and a major driver of forest disturbance and regrowth in Laos (Department of Forestry, 2018; Saphangthong and Kono, 2009). To reduce net carbon emissions, the Government of Lao PDR committed to increasing forest cover to 70% by 2020 (The Government of Lao PDR, 2005); however, this goal was not reached and has now been set to 2025. Accurate and timely monitoring of shifting cultivation is central to this commitment and to Laos's participation in REDD+. The current REDD+ reporting of Laos is based on land cover maps from 2005, 2010 and 2015 to generate the activity data (Department of Forestry, 2018). Such post-classification comparisons at five-year intervals are inadequate to map shifting cultivation.

Monitoring shifting cultivation is also valuable for understanding agriculture production and food security issues in Laos. Of relevance to the issue of shifting cultivation is that Laos ranks 87 of 117 countries on the 2019 Global Hunger Index (GHI) list with a score of 25.7 which is considered "serious hunger" on the GHI Severity Scale (Wiesmann, 2006; Von Grebmer et al., 2019). While over 80% of all arable land is used for rice, Lao rice farming is the least commercialized in the Lower Mekong (Manivong and Cramb, 2020). The lack of commercialization makes the production vulnerable to floods and droughts, which has hindered the creation of a reliable national rice surplus (Manivong and Cramb, 2020). Food security for a large proportion of the Lao population still depends on subsistence agriculture based on shifting cultivation (Roder, W., 2000; Heinimann et al., 2013). In 2011, about half of all villages in Laos cultivated upland rice under shifting cultivation (Epprecht et al., 2018). Especially in northern Laos, many villages devoted more than 75% of their agricultural land to grow upland rice under shifting cultivation, since it is difficult to develop alternatives of shifting cultivation due to the mountainous topography and low potential for irrigation development (Epprecht et al., 2018).

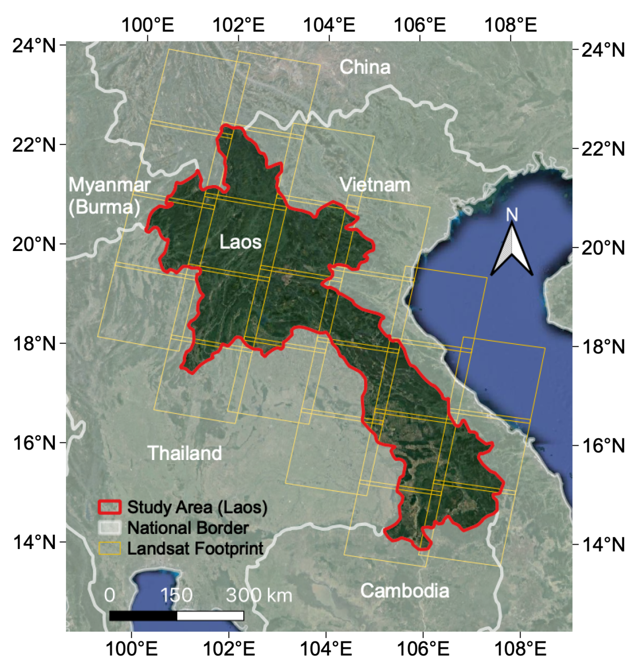

Fig. 1 Study area.

3 Method

3.1 Overview

All available Landsat Collection 1 surface reflectance data from 1987 to 2020 for the 24 Landsat scenes covering Laos were analyzed on Google Earth Engine. In our method (**Fig. 2**), forest disturbance is detected using Continuous Change Detection and Classification - Spectral Mixture Analysis (CCDC-SMA) (Chen et al., 2021) (**Section 3.2**). The time series of different types of forest disturbances and CCDC-SMA model fits were investigated (**Section 3.3**) in support of differentiating drivers of disturbance. Annual land cover maps were created to differentiate *Shifting cultivation* from *New Plantation* or *Deforestation* (**Section 3.4**). Object-based image analysis was applied to differentiate *Shifting cultivation* from large-scale natural disturbance, such as *Severe drought* (**Section 3.5**). Disturbance magnitude was used to differentiate *Shifting cultivation* from *Subtle disturbance*, such as pest damage and mild drought (**Section 3.6**). These different maps were combined to map shifting cultivation and other types of disturbance (**Section 3.7**). Following the creation of maps, the accuracy and areas of the various forest disturbances were estimated in a sampling-based approach (**Section 3.8**).

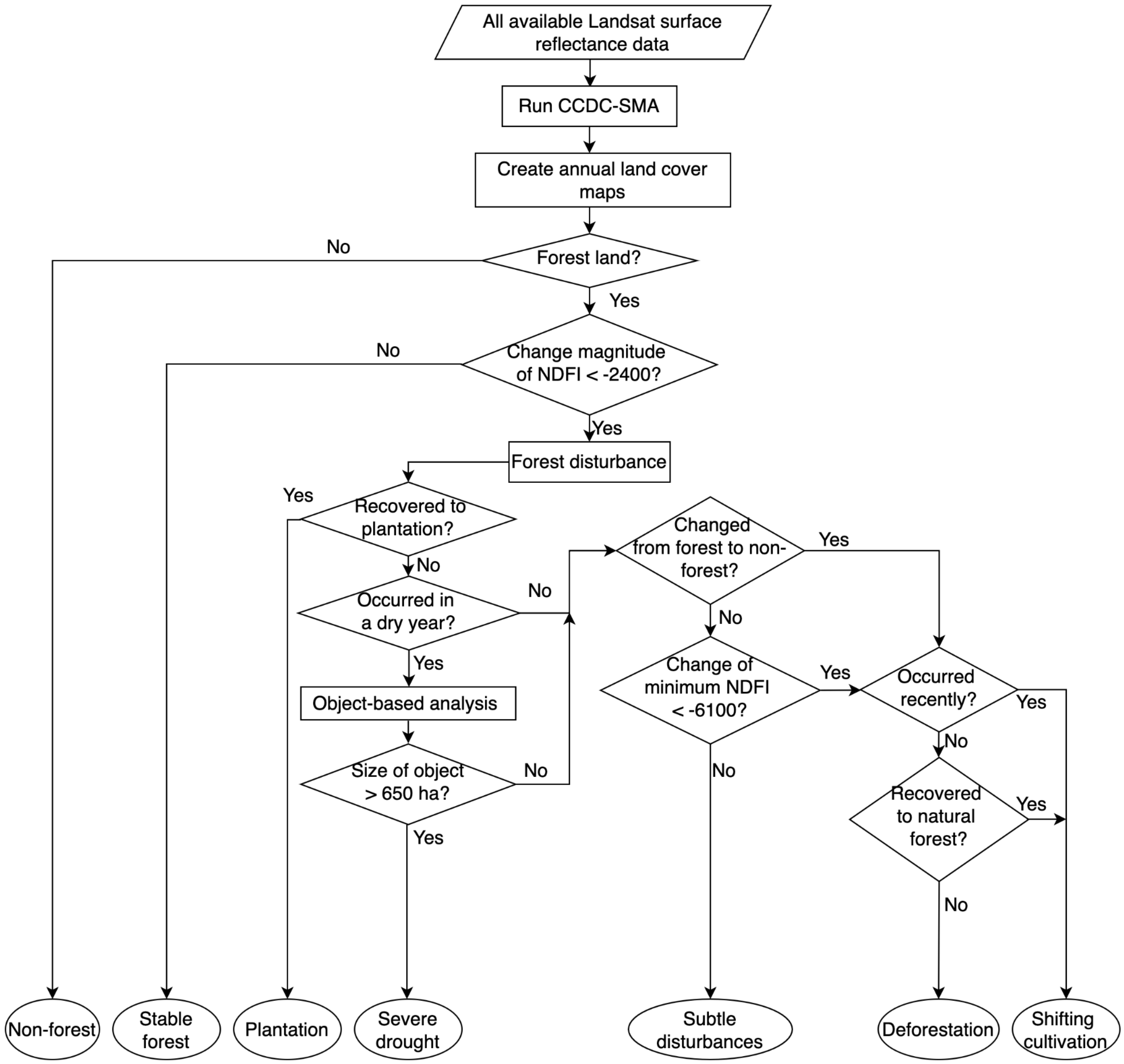

Fig. 2 Flowchart of the method. ("Recently" refers to the period 2015 - 2020.)

3.2 CCDC-SMA

CCDC-SMA, developed by Chen et al. (2021), combines Continuous Change Detection and Classification (CCDC (Zhu & Woodcock, 2014)) and Spectral Mixture Analysis (SMA) on GEE. CCDC-SMA uses Normalized Difference Fraction Index (NDFI) and the fraction of endmembers instead of the original spectral bands to detect breaks, since the SMA-derived indices are more sensitive to forest degradation (Chen et al., 2021; Bullock et al., 2020). Harmonic models are used to predict NDFI and fractions of endmembers for any given date. A model break is triggered if the predictions significantly deviate from the observations for a certain number (five in this step) of consecutive observations. Then, a new harmonic model is initiated. This process is conducted repeatedly from the start to the end of the time series.

The endmembers of green vegetation (GV), non-photosynthetic vegetation (NPV), soil, and cloud were collected in Landsat data for Laos. The endmember of shade is assigned to zeros at all bands. We created two image composites of Laos using the median of the spectral reflectance (one from the dry season and the other from wet season). In total, 16 subsets of image composites in 8 regions with different land cover types were used to extract endmembers. We used PySptools to facilitate the endmember extraction (Therien, 2018; Winter, 1999). Spectra of 5000 random sample points drawn from the two image composites were extracted and plotted in the spectral space. The pixels located at the extremes of the spectral space were identified as endmembers. Surface reflectance of the endmembers are shown in **Table 1** and **Fig. 3**. A linear spectral mixture model was used to calculate the fraction of endmembers. The fractions were constrained to be non-negative and sum to one. To evaluate the endmembers, RMSEs of the SMA model of image composites for seven selected years were calculated and examined (**Fig. 4** as an example). The RMSEs are all very low, indicating a good performance of the SMA model (**Table 2**).

Table 1 Surface reflectance of the endmembers collected in Laos (NIR: Near-infrared; SWIR: Short-wave infrared. The reflectance is scaled by 10,000).

Endmembers	Blue	Green	Red	NIR	SWIR1	SWIR2
GV	374	898	344	7456	2833	966
Soil	1817	1740	1818	3347	5647	5565
NPV	976	1553	2369	3660	5582	4323
Cloud	7984	8394	8445	6682	4574	3317
Shade	0	0	0	0	0	0

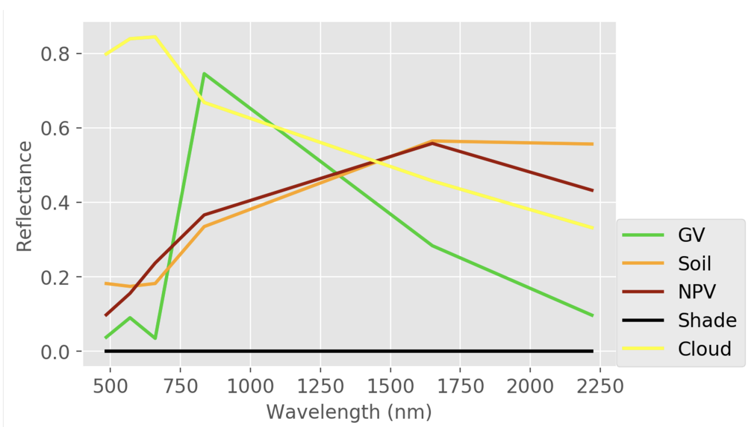

Fig. 3 Spectral reflectance of the endmembers.

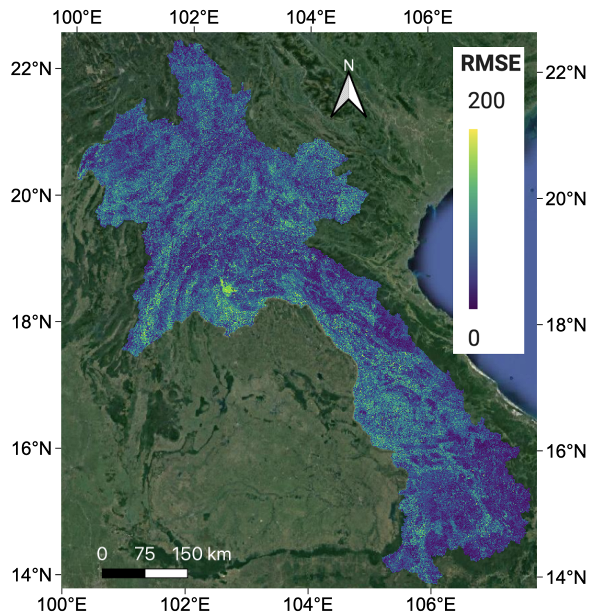

Fig. 4 RMSE of SMA model of dry season in 2020. (The reflectance is scaled by 10,000.)

Table 2 The mean of RMSE of the SMA model of seven selected years. (Scaled by 10,000.)

Year	1990	1995	2000	2005	2010	2015	2020
RMSE	73	82	68	74	74	56	57

After removing cloudy observations using the fraction of cloud, we ran CCDC-SMA on GEE by grid: The whole country of Laos was split into 19 grids and CCDC-SMA was run using the Landsat data in each grid. We used NDFI and the fraction of endmembers (except for cloud) as the inputs considered for finding breaks using the CCDC function in GEE. To facilitate land cover classification (**Section 3.6**), we also saved the coefficients from the harmonic regression for the original spectral bands. We used CCDC-SMA for temporal segmentation and detecting forest disturbances, and CCDC (with original bands) for land cover classification (similar to Chen et al., 2021), because using the SMA-derived indices are more sensitive to forest degradation (Chen et al., 2021), whereas using the original bands works better for classifying land cover in non-forest regions.

To determine the optimal threshold to classify breaks into disturbances and stable, we drew a simple random sample of 2500 units (pixels) and interpreted the time series of sample points into *Undisturbed forest*, *Forest disturbance* (including both natural and anthropogenic disturbance in this step) and *Non-forest*, by investigating Landsat and high-resolution images on Google Earth. Only the points with high-confidence interpretation were used in the later analysis. The change magnitude of NDFI (median of the observation minus the prediction for 5 consecutive observations) was tested to separate *Undisturbed forest* and *Forest disturbance*. The optimal threshold was found to be -2400 (**Fig. 5**).

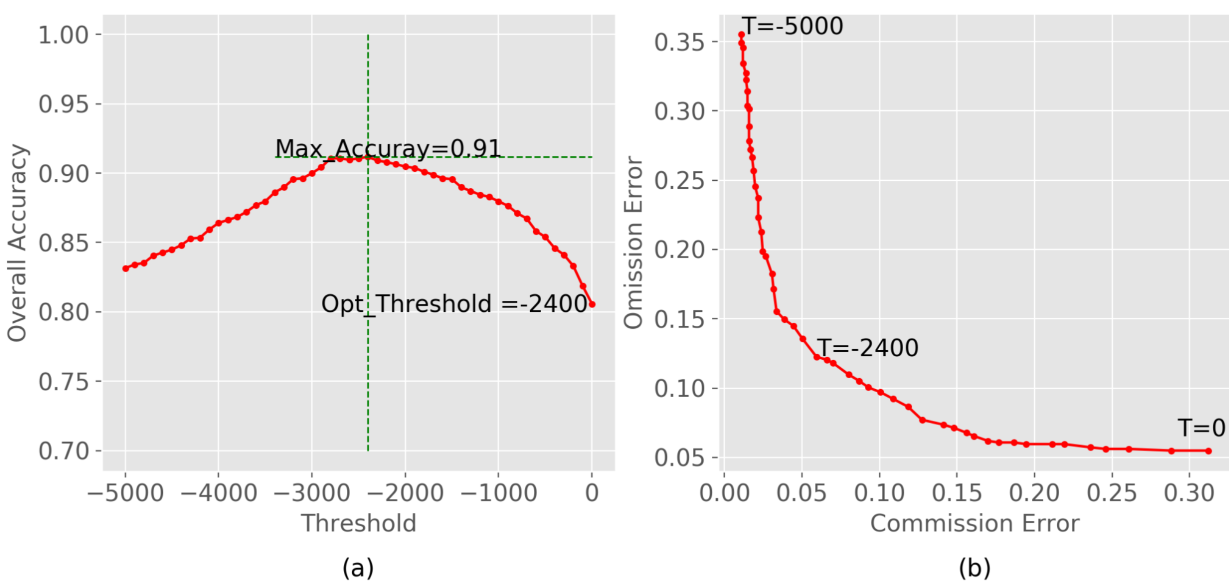

Fig. 5 Optimal threshold for the change magnitude used to classify breaks into *Forest disturbance* and *Undisturbed forest*. The plots show the accuracies and errors of these tests. (Max_Accuracy: maximum overall accuracy; Opt_Threshold: Optimal threshold; T: Thresholds)

3.3 Time series of different types of disturbance

The major types of forest disturbance in Laos are shifting cultivation, deforestation, drought and plantation. **Fig. 6 - 10** show the time series of these different types of disturbance. Shifting cultivation usually has several cycles of disturbance, although in some places only one cycle occurred. Each cycle started with a slash-and-burn event, followed by a short cropping period (typically one to two years), and a fallow period for vegetation to regrow. These stages of shifting cultivation can be observed in the time series of Landsat data (**Fig. 6**). Each slash-and-burn event results in a large and sudden decrease in NDFI. During the cropping period, NDFI is higher than the slash-and-burn stage and has a larger seasonality than the fallow period. When the land is left to regrow (fallow period), NDFI recovers to high values and low seasonality, as the land cover returns to forest. Forest to plantation (*New plantation*) shows a different pattern in the time series (**Fig. 7**). Although the clearing of a forest for plantation causes a large decrease in NDFI similar to shifting cultivation, the seasonality of a plantation is larger than that of a secondary forest in the fallow period of shifting cultivation. Thus, we can use the seasonality of the time segment after the disturbance to differentiate *Shifting cultivation* and *New plantation*. Similarly, the land cover after deforestation has different spectral-temporal signatures compared to the regenerated forest after slash-and-burn events, and thus differentiating *Shifting cultivation* from *Deforestation* can be achieved by classifying the land cover after a disturbance (**Fig. 8**). Severe drought leads to a time series similar to shifting cultivation with one slash-and-burn event **(Fig. 9)** but the spatial pattern is different. Also, severe drought results in an area of disturbance that is larger than that of slash-and-burn events. Thus, we can use an object-based analysis to separate *Severe drought* and *Shifting cultivation*. Subtle disturbance, such as selective logging and mild drought, result in more subtle decreases in NDFI than slash-and-burn (**Fig. 10**), which suggests that the magnitude of decrease in NDFI can be used for classification of disturbance types.

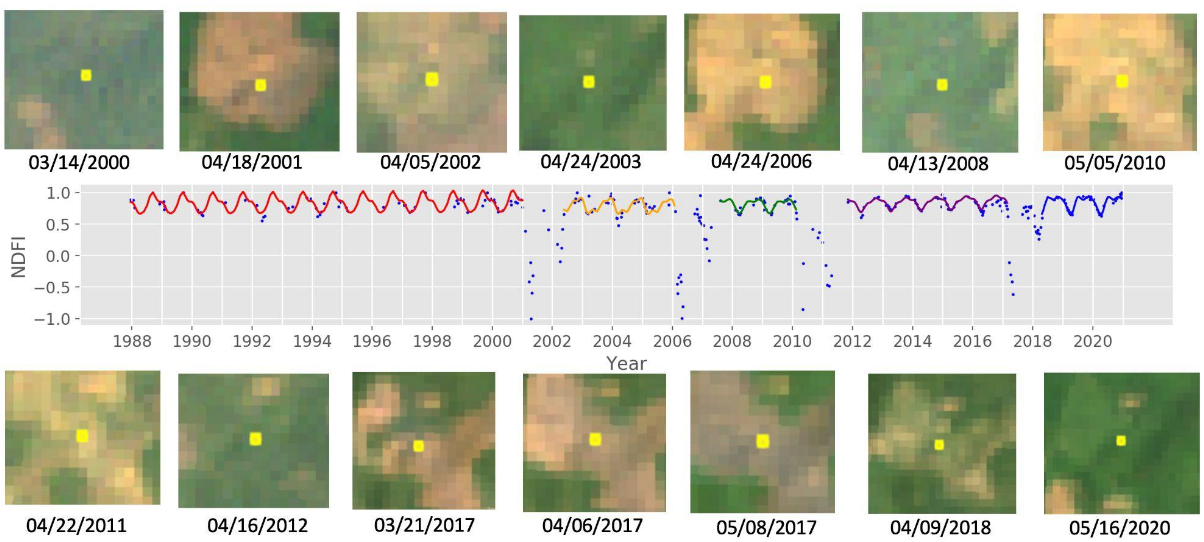

Fig. 6 Time series of an example of shifting cultivation. Slash-and-burn events occurred in 2001, 2006, 2010, and 2017. The Landsat images captured the events and the fallow periods. The three Landsat images in 2017 captured the “slash-and-burn” process: The images on 03/21 and 04/06 show the “slash” process and the image on 05/08 shows the “burn” process. (Example location: 20° 2' 14"N, 100° 50' 7" E. In the time series plot, the blue points are the Landsat observations, and the colored lines are the CCDC-SMA model fits, where different colors indicate different segments. In the Landsat images (Red-green-blue), the yellow squares show the pixel location.)

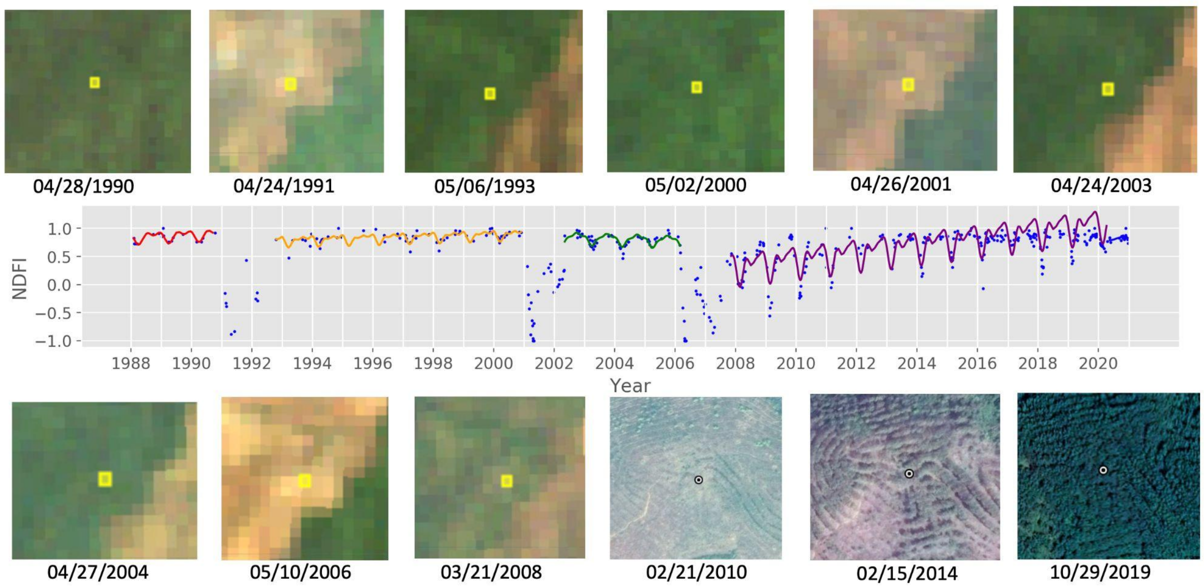

Fig. 7 Time series of an example that includes both shifting cultivation and forest to plantation. Clearing for shifting cultivation occurred in 1991 and 2001. In 2006, the land was cleared for rubber plantation. The Landsat images show the stages of shifting cultivation and the high-resolution images show the plantation. (Example location: 20°27'35"N, 101°24'50"E. In the time series plot, the blue points are Landsat observations, and the colored lines are the CCDC-SMA model fits, where different colors indicate different segments. In the Landsat images (Red-green-blue), the yellow squares show the pixel location. In the high-resolution images, the white circles show the center of the pixel.)

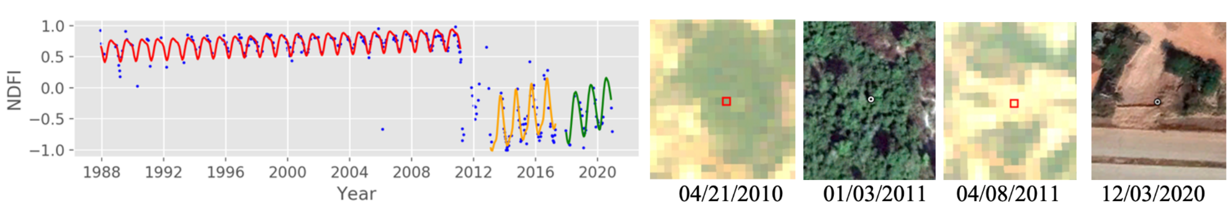

Fig. 8 Time series of an example of deforestation that occurred in 2011. Both the Landsat images and the high-resolution images show that the land cover was permanently converted from forest to non-forest. (Example location: 17°56'10"N, 102°40'45"E. In the time series plot, the blue points are Landsat observations, and the colored lines are the CCDC-SMA model fits, where different colors indicate different segments. In the Landsat images (Red-green-blue), the yellow squares show the pixel location.)

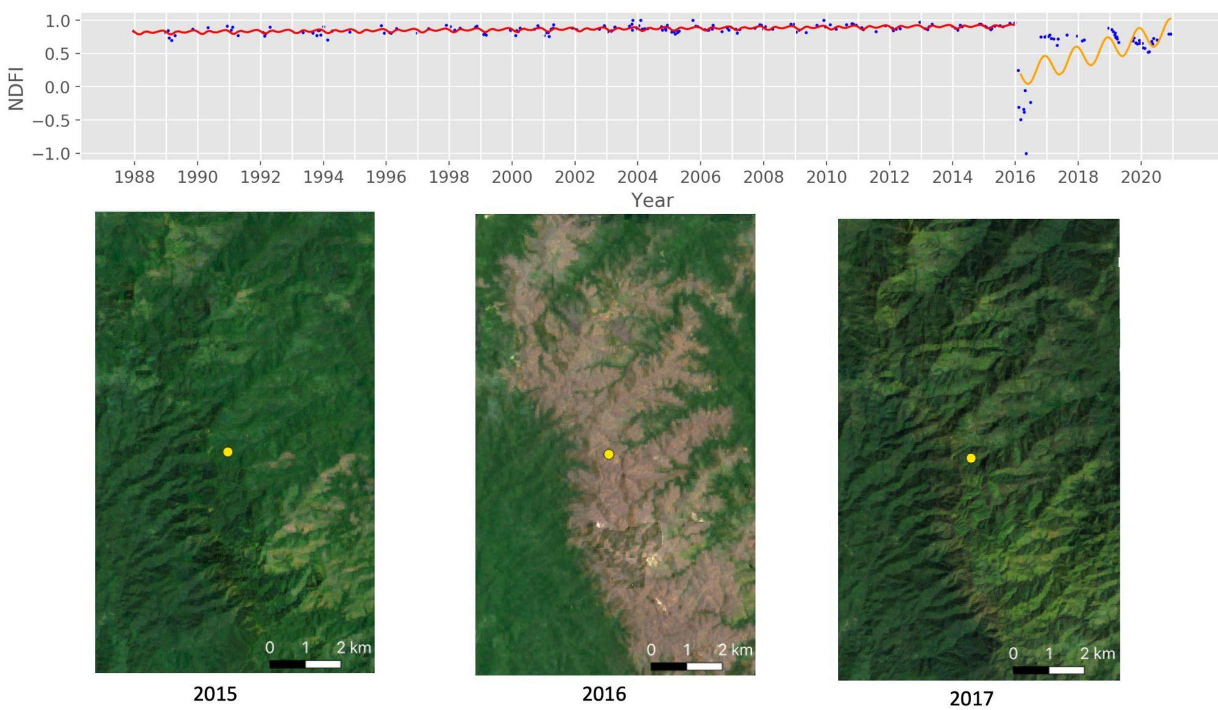

Fig. 9 Time series of an example of severe drought in 2016. The three Landsat images were acquired before, during and after the disturbance. (Example location: 20°17'8"N, 103°18'25"E. In the time series plot, the blue points are Landsat observations, and the colored lines are the CCDC-SMA model fits, where different colors indicate different segments. In the Landsat composites (Red-green-blue), the yellow points show the pixel location. The reddish-brown region was affected by severe drought.)

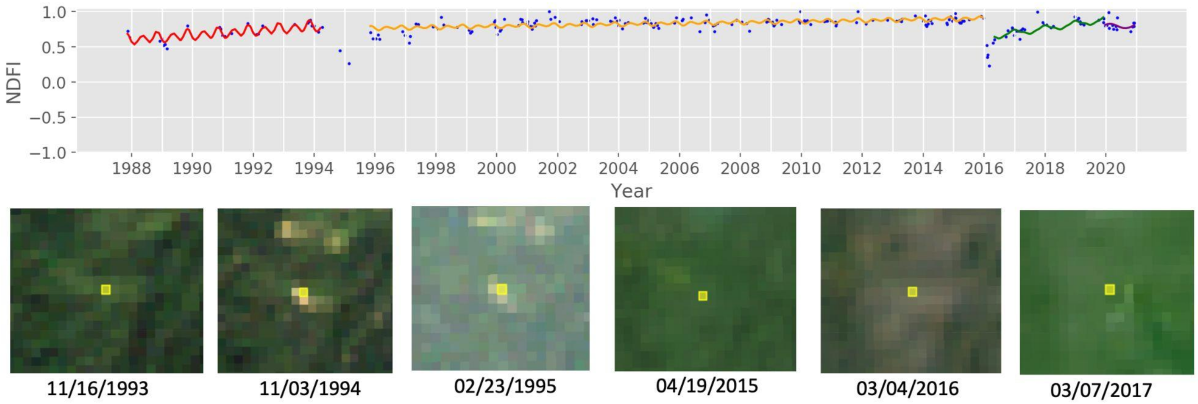

Fig. 10 Time series of an example of subtle disturbance, such as selective logging or mild drought. Selective logging occurred in November 1994, and a mild drought affected this location in 2016. (Example location: 20°17'40"N, 103°10'30"E. In the time series plot, the blue points are Landsat observations, and the colored lines are the CCDC-SMA model fits, where different colors indicate different segments. In the Landsat images (Red-green-blue), the yellow squares show the pixel location.)

3.4 Land-cover-based monitoring

To classify disturbance types, annual land cover maps for Laos were created. First, we collected training data for the following land cover classes: *Forest, Plantation, Agriculture, Shrub or grass, Wetland or water* and *Non-vegetated*. We interpreted the land cover in 2017 for the 2500 random training points described in **Section 3.2**. Only the points with high-confident interpretation and stable land cover between 2012 to 2020 were included in the training data. After an initial test of classification, we found that plantations and dry forest were not mapped well in some regions, and thus we augmented the training points by collecting an additional 1799 training points in places where high-resolution (high-res) images are available in Google Earth.

A total of 3769 training points (1970 from random selection and 1799 from selection in areas of high-res coverage) were used in the classification. Second, we ran CCDC with the original bands from 1987-2020. Third, we trained a random forest classifier using the CCDC coefficients and training data to classify the time series segments. Each classified segment is continuous in time and can be transformed into maps at any discrete time interval.

An important difference between the method presented here and the routine method of making maps from CCDC (e.g. Tang et al. (2021) and Arévalo et al. (2019)) is an additional step of land cover classification at the model breaks between different segments, which is required to detect shifting cultivation. As mentioned, CCDC makes a continuous prediction of reflectance; the prediction halts or "breaks" when the observations in the time series behave differently than the predicted. The years between a break and the initiation of a new model are referred to as "break years" in this paper. Classifying the land cover during break years is essential for monitoring shifting cultivation. Taking the shifting cultivation in **Fig. 6** as an example, the segments of the fallow periods were all classified as forest. If land cover classification in the break years is ignored, the land cover of this pixel for the whole time would be classified as forest, and the temporary forest-to-agriculture change associated with shifting cultivation would be omitted in the annual land cover maps. To identify the land cover in the break years, we created image composites using the median reflectance of the original bands from February to May. This period was chosen because the slash-and-burn events usually happen in February to May, and February to April is the dry season of Laos, which is less affected by clouds. We used the median composites and the training data described above to classify the land cover in break years. Finally, annual land cover maps from 1990 to 2020 were created by combining the segment classification results and the land cover classification in break years (**Fig. 11** as an example).

Land-cover change was one of the rules used to determine disturbance type. If the land cover changed from *Forest* to *Plantation*, the disturbance type was *New plantation*. If the land cover changed from *Forest* to permanent *Non-forest*, the disturbance type was *Deforestation*. If the land cover temporarily changed from *Forest* to *Agriculture* or *Shrub*, the disturbance was *Shifting cultivation*.

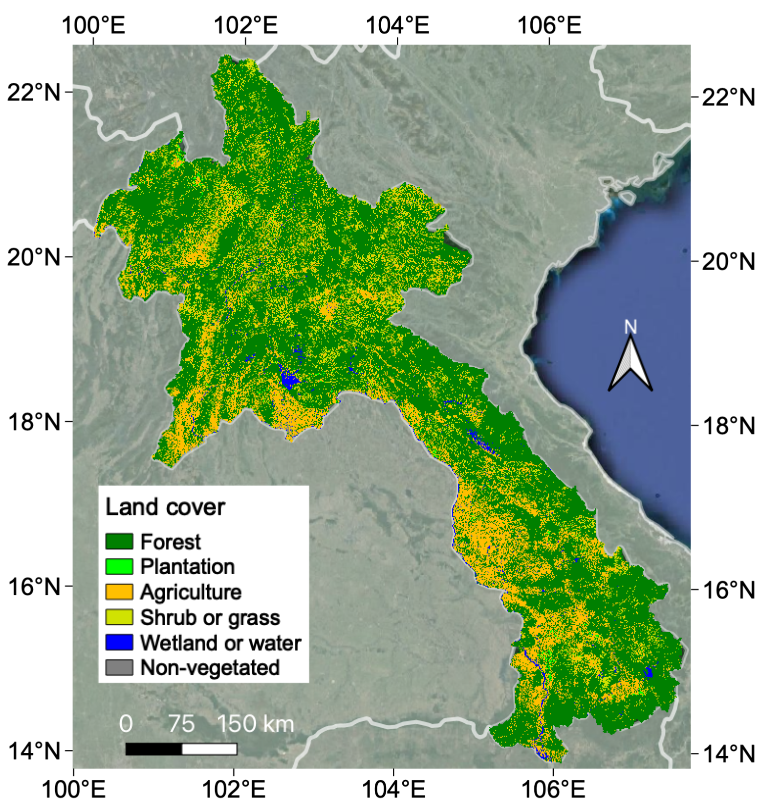

Fig. 11 Land cover map of Laos in 2020 as an example of the annual land cover maps of 1990 - 2020.

3.5 Object-based image analysis

Object-based image analysis has traditionally been mostly used in land cover classification (Costa et al., 2017; Belgiu and Csillik, 2018; Toure et al., 2018; Rendenieks et al., 2020) and less so for attributing change (Hermosilla et al., 2015; Yu et al., 2016). As we mentioned in **Section 3.3**, here we use object-based image analysis to differentiate *Shifting cultivation* from *Severe drought*. We used the Palmer Drought Severity Index (PDSI) to identify the dry years. PDSI uses precipitation and temperature data to estimate the severity of dry or wet spells of weather (Palmer, 1965). Positive values denote a wet spell and negative denote a dry spell. We calculated annual PDSI of Laos using the TerraClimate data (Abatzoglou et al., 2018) **(Fig. 12)**. PDSI < -2 indicates moderate to extreme drought (Wells et al., 2004). Years with PDSI < -2 are considered as dry years in this study.

Object-based image analysis was applied to the annual forest disturbance map (**Section 3.2**) for all the dry years. Pixels of *Forest disturbance* were aggregated to objects based on their connectedness and then the sizes of the objects were calculated (**Fig. 13 (a)**). We interpreted the disturbance type (*Shifting cultivation* or *Severe drought*) of 411 pixels located in different objects by investigating time series and imagery of Landsat, and high-resolution imagery on Google Earth if available. After summarizing the sizes of these objects associated with the 411 example pixels in a histogram (**Fig. 13 (b)**), we determined that objects larger than 650 ha were affected by severe drought. Applying this rule to the objects created in the OBIA, we identified objects as *Severe drought* in the dry years.

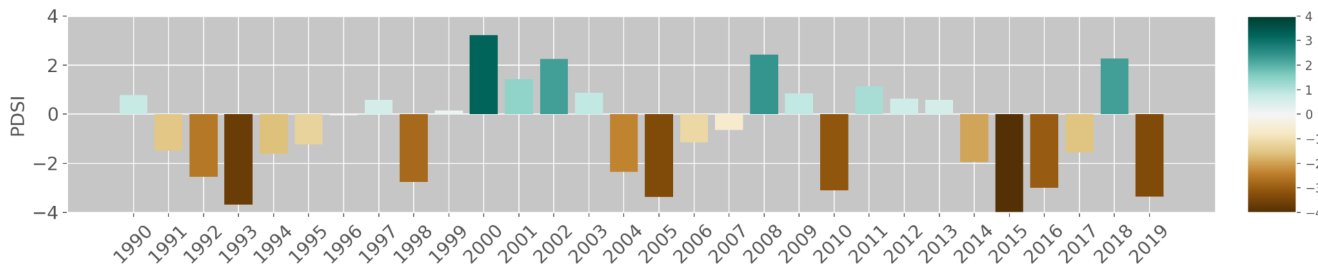

Fig. 12 Annual Palmer Drought Severity Index (PDSI) for Laos calculated from the TerraClimate data (Abatzoglou et al., 2018).

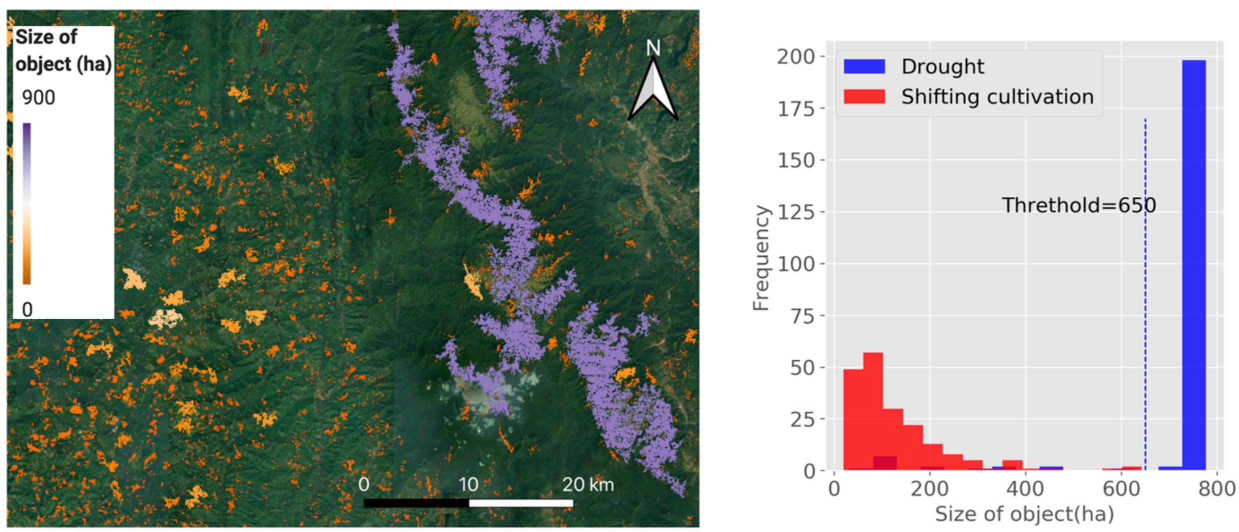

(a) (b)

Fig. 13 (a): Size of objects identified as *Forest disturbance*; (b): Histogram of the size of objects of *Severe drought* and *Shifting cultivation*.

3.6 Disturbance-magnitude-based monitoring

A further process for attributing disturbance is calculating the magnitude of disturbance. Two methods of calculating magnitude of disturbance to separate between *Shifting cultivation* and *Subtle disturbance* were tested: (1) the default change magnitude in CCDC-SMA: median of the observed NDFI minus the prediction for the 5 consecutive observations following a break; and (2) the minimum NDFI in the break year minus the NDFI before the break (called "disturbance magnitude" to distinguish from the default change magnitude). To determine the effectiveness of the two methods, we interpreted the disturbance type of the sample points labeled as *Forest disturbance* (described in **Section 3.2**). The points interpreted as *Shifting cultivation* and *Subtle disturbance* were used in this test. Since few observations of *Subtle disturbance* were identified, we collected an additional 148 points of *Subtle disturbance*. Using these points, we tested different thresholds and the two different methods of calculating magnitude of disturbance mentioned before to differentiate *Shifting cultivation* and *Subtle disturbance*. The test showed that the second method (maximum overall accuracy of the tests is 94%) performed better than the first one (maximum overall accuracy of the tests is 81%). The optimal threshold of disturbance magnitude to classify *Shifting cultivation* and *Subtle disturbance* is -6100 (**Fig. 14**).

Based on our visual examination, we found omissions of *Shifting cultivation* in the maps due to missed breaks in the CCDC-SMA model, especially in the early years when the data density is relatively low. To solve this problem, we set the number of consecutive observations to three. To speed up the computation and save storage, only the break year and the magnitude of NDFI was saved. Similarly, we calculated the disturbance magnitude, and detected places with disturbance magnitude < -6100 as *Shifting cultivation*. We found that by combining the runs of the model with the number of consecutive observations set to three and five, the detected *Shifting cultivation* is better than using either of them alone. Thus, if either one detected *Shifting cultivation*, it is labeled as *Shifting cultivation* in the final map.

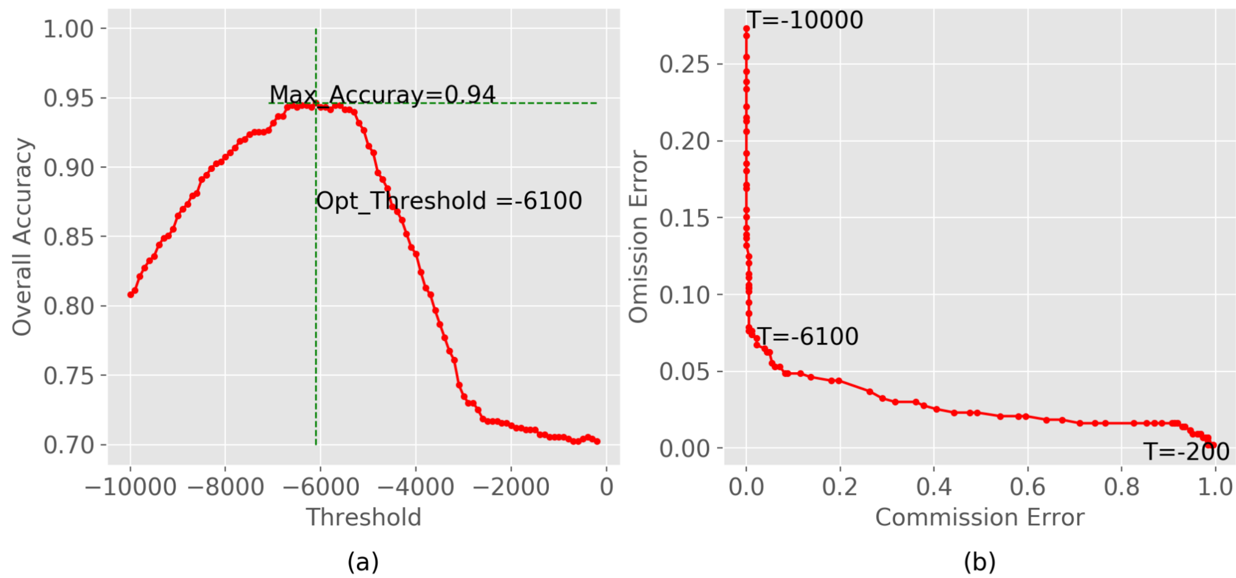

Fig. 14 Optimal threshold of disturbance magnitude to differentiate *Shifting cultivation* and *Subtle disturbance*. The plots show the accuracies and errors of testing different thresholds. (Max_Accuracy: maximum overall accuracy of the tests; Opt_Threshold: Optimal threshold; T: Thresholds)

3.7 Combining maps

The land-cover maps, object-based maps, and disturbance-magnitude maps were combined following the workflow in **Fig. 2**. First, we used the land cover maps to determine whether the disturbance was caused by conversion of forest to plantation. Second, if the disturbance was not plantation-driven and occurred in a dry year, we applied the severe drought mask created from OBIA to map areas of *Severe drought*. If the disturbance was neither drought- or plantation-driven, we investigated if the land cover changed from forest to non-forest (except for water) and back to forest, in which case we assumed the presence of *Shifting cultivation*. *Shifting cultivation* was also detected if the land cover remained forest and the disturbance magnitude exceeded the threshold. *Deforestation* was mapped if the disturbance happened in or before 2015 and the land cover remained non-forest after the disturbance. Further, we mapped a disturbance as *Shifting cultivation* rather than *Deforestation* if the disturbance happened after 2015 and the disturbance magnitude exceeded the threshold even if the land cover had not recovered to forest. This is because *Shifting cultivation* affects a much larger area than *Deforestation* in Laos, and hence is more likely to occur. Conversion of forest to water was labeled *Deforestation*. To avoid omitting the edge of *Shifting cultivation*, pixels within a 2-pixel buffer of *Shifting cultivation* and mapped as *Forest disturbance* were labeled *Shifting cultivation*. Finally, based on these rules, we created annual maps from 1991-2020 of *Shifting cultivation, Deforestation, Forest, New plantation, Plantation, Severe drought, Subtle disturbance*, and *Non-forest*.

3.8 Accuracy assessment

Following the guidelines recommended in the remote sensing literature (Olofsson et al. 2014), we drew a sample of pixels from the study area and observed reference conditions in satellite data at sample locations to assess the accuracy of the maps. To design an efficient sampling design, we created strata based on the annual maps (**Section 3.7**) for the whole study period (1991-2020) (**Fig. 19**). The definitions of the strata are:

- *Stable forest*: Stable forest pixels during the study period, without significant anthropogenic disturbances. Forests that only have natural disturbance, such as drought, were still mapped as stable forest.

- *Non-forest*: Non-forest pixels during the study period.
- *Shifting cultivation*: Pixels that have experienced shifting cultivation at any point during the study period.
- *New plantation*: Pixels that changed from forest to plantation at any point during the study period.
- *Deforestation*: Pixels that had permanent conversion from forest to non-forest (except for plantation) at any point during the study period. Land cover remained non-forest after disturbance for at least 5 years and has never recovered to forest.

The weight of the *Shifting cultivation* stratum was 36% (i.e. shifting cultivation affected 36% of Laos 1991-2020. The weights of all strata presented in the column of "Map area proportion" in **Table 3**). Stratified random sampling is common in land change studies as it ensures sufficient sampling of rare change classes (Olofsson et al., 2013). Here, because the *Shifting cultivation* stratum has such a large weight, we decided to use simple random sampling. The benefit of simple random sampling is the ability to use the same post-stratified estimator for area and accuracy estimation even if the stratification is altered after sampling (Stehman, 2013; Olofsson et al., 2020).

As recommended by Olofsson et al. (2014), the sample size was determined by solving the variance estimator for n under simple random sampling and specifying a target margin of error. A margin of error of 30% at the 95% confidence level, which is the target for estimating forest change suggested by the Forest Carbon Partnership Facility (FCPF, 2020), a World Bank funded REDD+ program that Laos participated in, yields a sample size of $n = 79$ if targeting shifting cultivation, and $n = 855$ if targeting deforestation. Based on these calculations, we draw a sample of 1,000 units (each unit is a Landsat pixel) under simple random sampling with the aim of estimating both shifting cultivation and deforestation with a margin of error of 30%.

Time series of Landsat data were extracted for each of the 1000 sample units and interpreted by two interpreters using the AREA2 tools (Arevalo et al., 2020). The interpreters were asked to interpret the reference class of the whole time series and the confidence level of their interpretation. If shifting cultivation happened in the study period, the interpreters recorded the number of the slash-and-burn events and the year of each event. For each sample unit, the interpreters examined time series of Landsat observations of NDFI, fraction of endmembers (GV, NPV, Soil, Shade), NIR, SWIR1, NDVI (Normalized Difference Vegetation Index) (Carlson et al., 1997), NBR (Normalized Burn Ratio) (Roy et al., 2006), and NDMI (Normalized Difference Moisture Index) (Jin and Sader, 2005) on GEE. The interpreters also examined Landsat imagery on GEE and high-resolution imagery on Google Earth to determine the reference conditions and disturbance year (**Fig. 15**). The two interpreters first collected reference observations independently and then compared their observations. Each sample unit was interpreted at least twice. Sample units with different interpretations were discussed in a group effort to provide an agreed-upon label. A sample unit was discarded if the disagreement could not be reconciled; a total of 23 sample units were discarded which yielded a final sample size of 977 units.

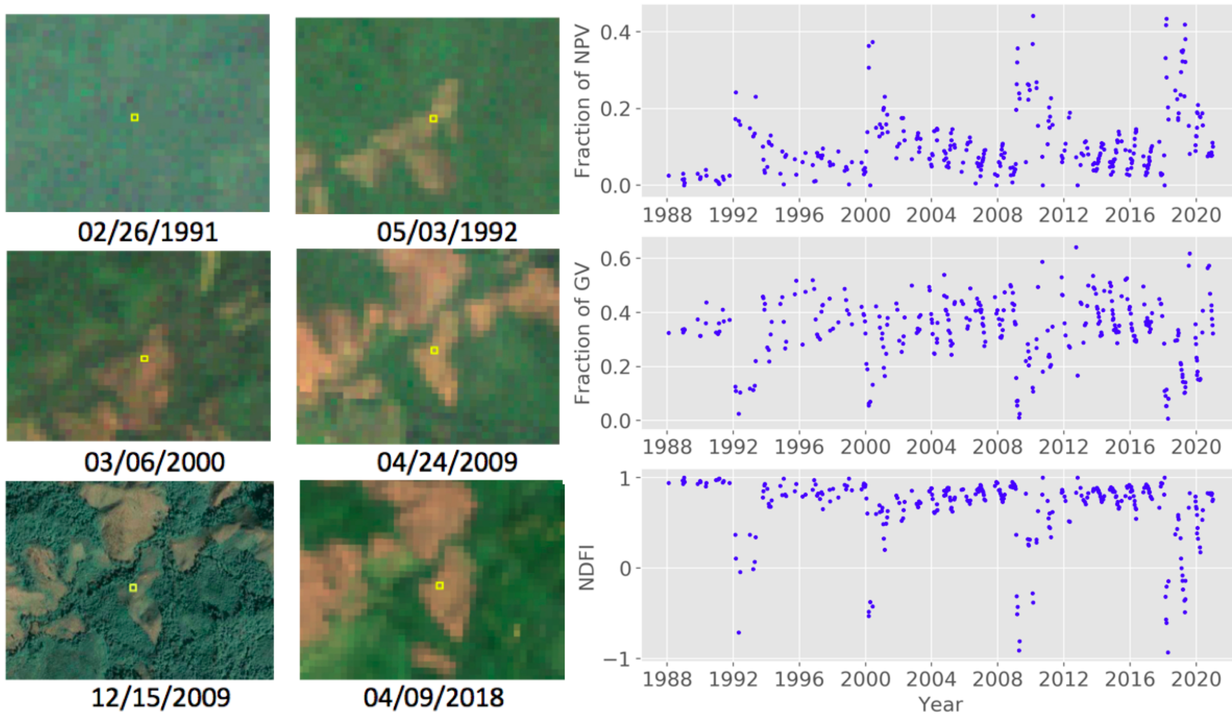

Fig. 15 Reference data collection. This sample unit was interpreted as "*Shifting cultivation*". The number of slash-and-burn events is 4, and the year of events are 1992, 2000, 2009, and 2018. (Sample unit location: 20°35'54"N, 101° 0'11"E. The images on the left side are Landsat images and a high-resolution image on Google Earth. The plots on the right side are Landsat observations of fraction of NPV, fraction of GV and NDFI. All these time series show significant change in each slash-and-burn event.)

3.9 Post-processing

After a preliminary inspection of the maps, we found commission errors for *Shifting cultivation* caused by drought in some regions. Thus, in the dry years, we added an extra rule to reduce such commission errors: If the minimum NDFI one year after a break minus the NDFI before the break was less than 0.3, the break was mapped as *Drought*. The rule was based on the assumption that forests affected by drought recover faster than shifting cultivation. Also, we found commission errors of *Shifting cultivation* due to misclassifying plantations as forest after disturbance. Thus, we added more training data of plantations in these regions and updated the land cover map to reduce the commission errors. After these two post-processing steps, the user's accuracy of shifting cultivation increased from 78.0% to 80.2%.

4 Results

4.1 Annual disturbance type

We created annual disturbance maps from 1991-2020 of *Forest, Plantation, Non-forest, Shifting cultivation, Deforestation, New plantation, Severe drought* and *Subtle disturbance* (**Fig. 16** shows an example map in 2016). In the annual maps, *Shifting cultivation* refers to the slash-and-burn events that occurred in a certain year. *New plantation* refers to land cover change from forest to plantation in a certain year. *Plantation* refers to plantations that were previously established. *Severe drought* refers to drought events that occurred on a large-scale. *Subtle disturbance* include pest damage, mild drought, or subtle anthropogenic disturbances, such as selective logging. A map of the first year of shifting cultivation was created, which shows the expansion of shifting cultivation from places adjacent to permanent agriculture to places close to stable forests in some regions (**Fig. 17**). We calculated the areas of the disturbance classes based on pixel counting from the annual maps (**Fig. 18**), and it shows that shifting cultivation is the major disturbance type for every year.

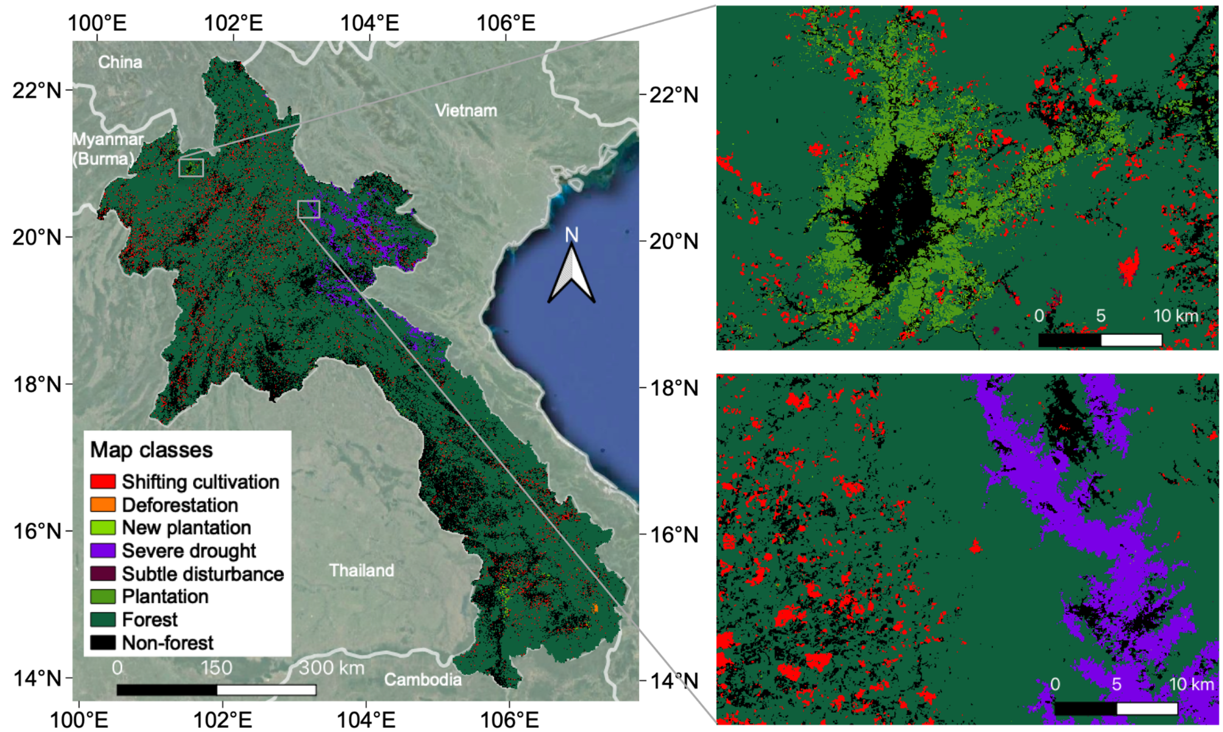

Fig. 16 Disturbance map of Laos in 2016 as an example of annual disturbance maps from 1991-2020.

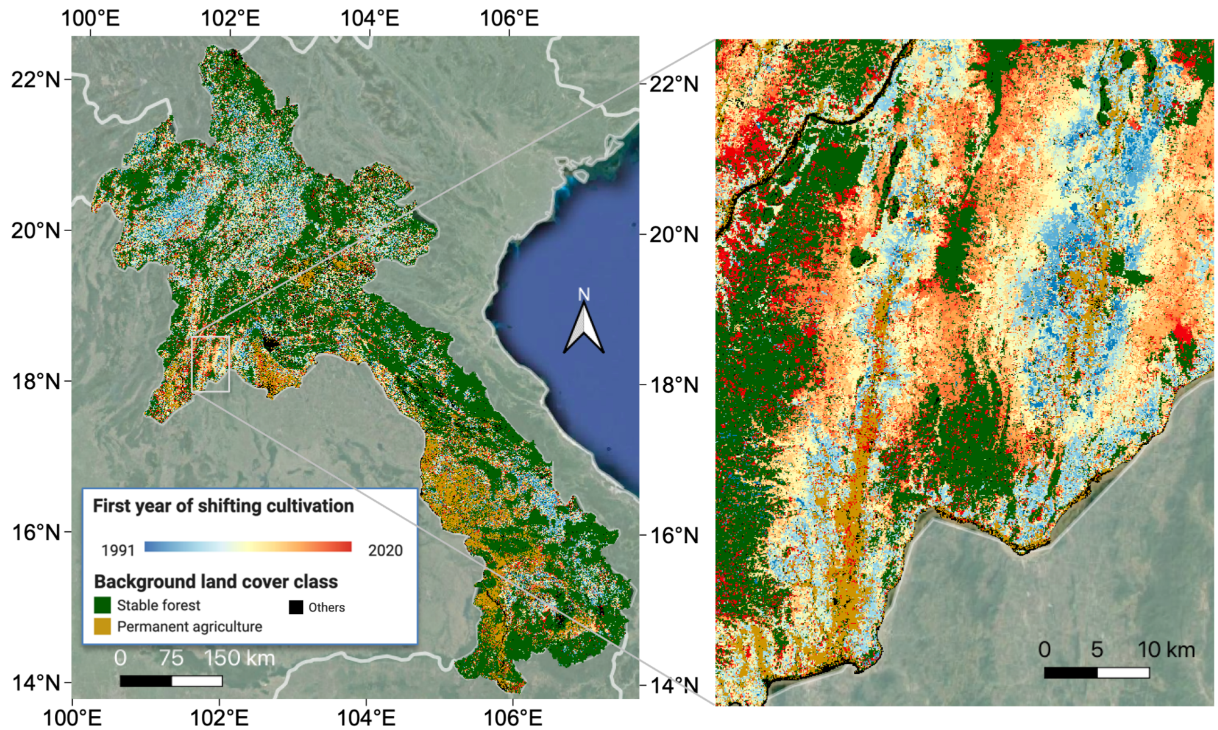

Fig. 17 First year of shifting cultivation in Laos. Places without shifting cultivation were mapped as *Stable forest, Permanent agriculture* and *Others*. In the magnified view of a region, shifting cultivation expanded from places adjacent to permanent agriculture to places close to stable forest.

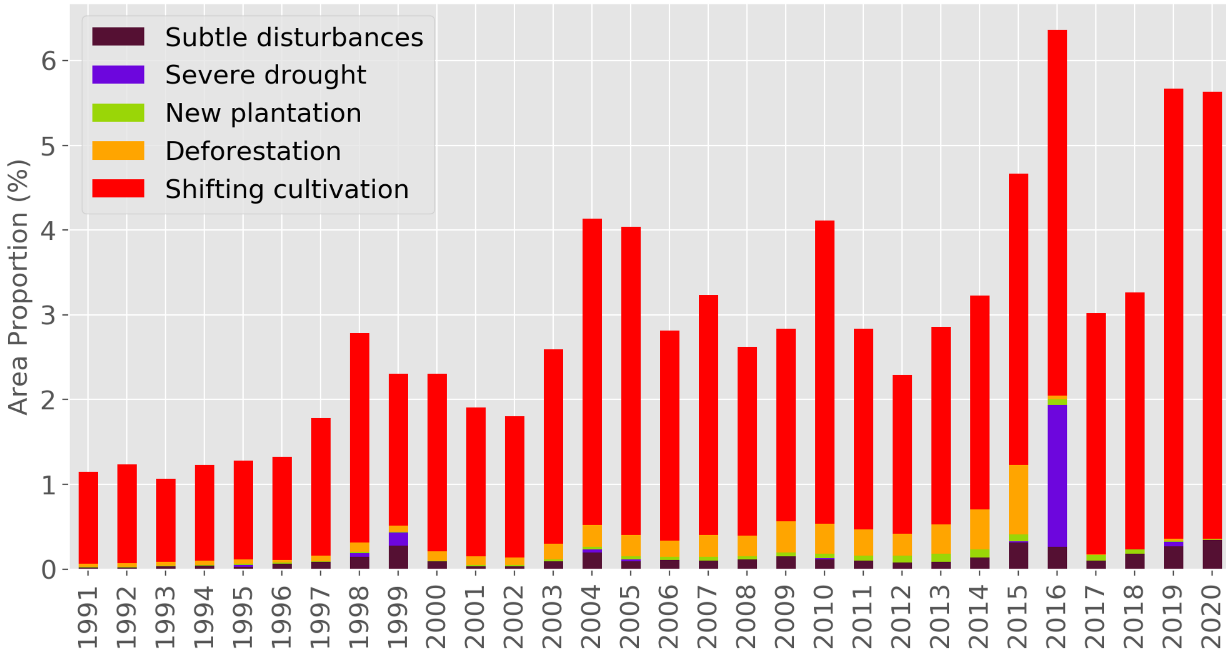

Fig. 18 Annual area proportion of different disturbance types calculated from the map. The histograms are stacked, meaning that the total height of the bar for each year is the sum of the area proportions of all five types of disturbance for this year.

4.2 Accuracies and area estimates for the study domain

Based on the annual maps, an aggregated disturbance map of *Stable forest*, *Non-forest*, *Shifting cultivation*, *Deforestation* and *New plantation* for the whole study period was created (**Fig. 19**). The definitions of these classes are explained in **Section 3.8**. We used the reference data to conduct an accuracy assessment of the aggregated map and area estimation of the classes (**Table 3** and **Table 4**). Shifting cultivation was the major disturbance, affecting 32.9% ± 1.9% of Laos (95% confidence interval) over the period 1991-2020. *Shifting cultivation* was mapped at high accuracy: the producer's accuracy is 87.7%; the user's accuracy is 80.2%; and the margin of error of the area estimates is 5.9%. The errors of *Shifting cultivation* are mostly due to the misclassification between *Shifting cultivation* and *Stable forest* class (note that *Stable forest* class includes natural disturbances) (**Table 3**). *Stable forest* was also mapped at high producer's (89.6%) and user's accuracy (93.0%). The accuracy of *Deforestation* is relatively low due to misclassification between *Shifting cultivation* and *Deforestation*. *Plantation* is a very small class with relatively few observations in the sample results which results in rather uncertain area estimates. The overall accuracy of the map is (84.5%). The margins of error of area estimates are below 25% for all classes except for *New plantation*. The mapped area of *Shifting cultivation* is close to the sampling-based estimates, although slightly larger than the upper bound of the 95% confidence interval (**Fig. 20**). The mapped areas of other classes are all within the 95% confidence interval of the area estimates (**Fig. 20**).

If combining all the disturbance classes (*Shifting cultivation*, *New plantation*, and *Deforestation*) into one *Forest disturbance* class, the area estimate of the *Forest disturbance* class is 88,555 ± 4,315 km^2 (38.4% ± 1.9%). The user's and producer's accuracy of the *Forest disturbance* class is 84.2% and 90.6%, respectively. The margin of error of the area estimate of *Forest disturbance* is 4.9%. The overall accuracy of this combined map (*Stable forest, Non-forest* and *Forest disturbance*) is 87.7%.

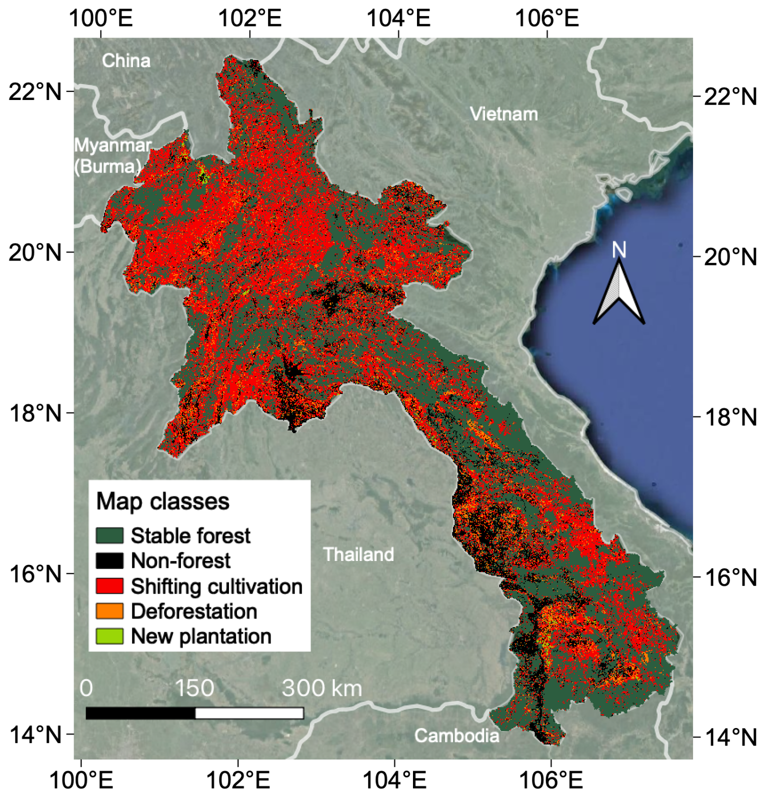

Fig. 19 Map of *Stable forest*, *Non-forest*, *Shifting cultivation*, *Deforestation* and *New plantation* of Laos during 1991-2020.

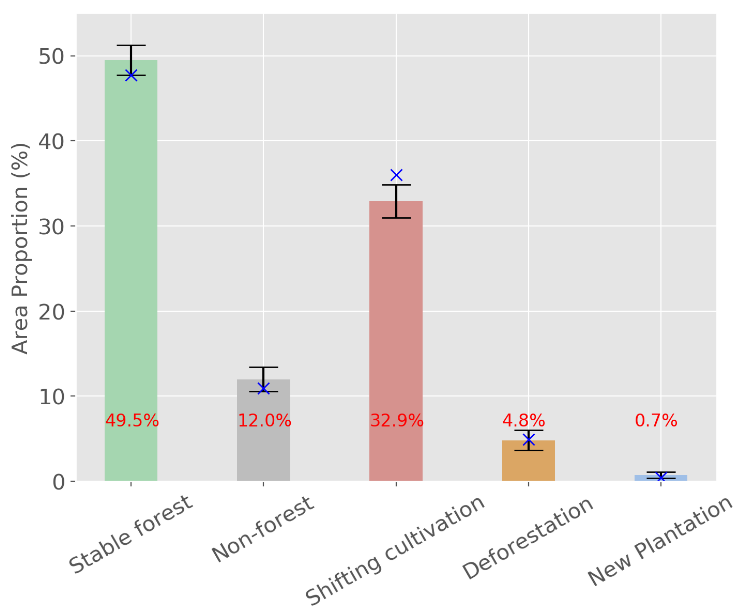

Fig. 20 Sampling-based area estimation (expressed in proportion) of *Stable forest*, *Non-forest*, *Shifting cultivation*, *Deforestation* and *New plantation* of Laos during 1991-2020. (Colored bars and numbers in red: The area estimates in proportion; black bar: error bar showing uncertainty of the estimates; blue cross: mapped area).

Table 3 Confusion matrix expressed in sample counts, mapped area and mapped area proportions of the classes.

		Reference							
		Stable forest	**Non-forest**	**Shifting cultivation**	**Deforestation**	**New plantation**	**Total**	**Map area (km^2)**	**Map area proportion**
Map	**Stable forest**	439	6	26	1	0	472	109934	47.7%
	Non-forest	14	78	2	5	1	100	25154	10.9%
	Shifting cultivation	30	16	264	17	2	329	82966	36.0%
	Deforestation	4	14	15	29	0	62	11382	4.9%
	New plantation	0	0	0	0	14	14	969	0.4%
	Total	487	114	307	52	17	977	230405	100.0%

Table 4 Sampling-based area estimates, accuracies and uncertainties of the classes.

Class name	Stable forest	Non-forest	Shifting cultivation	Deforestation	New Plantation	Total
Area estimates (km^2)	114069 ± 4067	27623 ± 3257	75887 ± 4460	11101 ± 2712	1725 ± 855	230405
Area proportion	49.5% ± 1.8%	12.0% ± 1.4%	32.9% ± 1.9%	4.8% ± 1.2%	0.7% ± 0.4%	100%
Margin of error	3.6%	11.8%	5.9%	24.4%	49.5%	
User's accuracy	93.0%	78.0%	80.2%	46.8%	100.0%	
Producer's accuracy	89.6%	71.0%	87.7%	48.0%	56.2%	
Overall accuracy						84.5%

4.3 Accuracies and area estimates of shifting cultivation by period

We estimated the area of disturbance caused by shifting cultivation for 5-year periods from 1991 to 2020 (**Fig. 21** and **Table 5**). Any slash-and-burn event occurring in a certain 5-year period was included in the area estimates for that period. Specifically, sites cultivated multiple times in different periods were included in the 5-year estimates multiple times, whereas for sites cultivated multiple times within the same period, only one time is included in the area estimates. Therefore, the area estimates show how much area is affected by slash-and-burn events for each period.

The areas of slash-and-burn events are estimated with low uncertainty. For all 5-year periods, the overall accuracies of the slash-and-burn by period are all higher than 92%, and the margins of error all less than 17%. Except for the first and the last period, the mapped areas are all within the 95% confidence intervals which suggests that the maps exhibit a low level of area bias. For the first period, the mapped area was lower than the sampling-based estimates, because the Landsat density is relatively low in the first period, which causes high omission errors of slash-and-burn events. The mapped area was higher than the sampling-based estimates for the last period, because the algorithm misclassified some regions affected by drought in 2016 and 2019 as *Shifting cultivation*. The user's and producer's accuracies for 2001-2005, 2006-2010, and 2011-2015 are all higher than 72%. For the first two periods, the producer's accuracy was low due to relatively low Landsat data density. The producer's accuracy of the period 2016-2020 is high (89%), whereas the user's accuracy of the 2016-2020 time period is lower (70%) due to the misclassification between *Drought* and *Shifting cultivation*.

The GEE codes and apps in this study are hosted on https://github.com/shijuanchen/shift_cult .

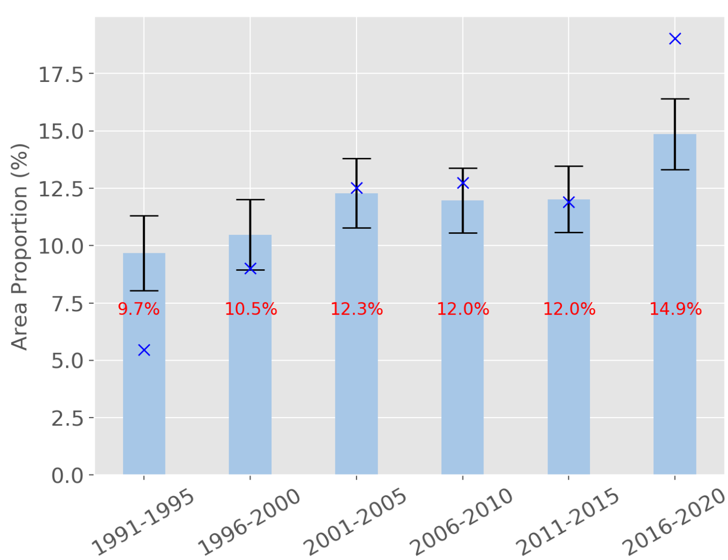

Fig. 21 Area estimates of slash and burn events by period during 1991-2020. (Colored bars and numbers in red: The area estimates in proportion; black bar: error bar showing uncertainty of the estimates; blue cross: mapped area)

Table 5 Sampling-based area estimates, accuracies and uncertainties of slash and burn events for the 5-year periods during 1991-2020.

Period	**1991-1995**	**1996-2000**	**2001-2005**	**2006-2010**	**2011-2015**	**2016-2020**
Area estimates (km^2)	**22307 ± 3757**	**24124 ± 3532**	**28295 ± 3480**	**27582 ± 3246**	**27687 ± 3337**	**34241 ± 3545**
Area proportion	**9.7% ± 1.6%**	**10.5% ± 1.5%**	**12.3% ± 1.5%**	**12.0% ± 1.4%**	**12.0% ± 1.5%**	**14.9% ± 1.5%**
Margin of errors	**16.5%**	**14.3%**	**12.2%**	**11.7%**	**12.5%**	**10.1%**
User's accuracy	**68.5%**	**68.0%**	**72.2%**	**73.9%**	**72.8%**	**69.6%**
Producer's accuracy	**38.6%**	**58.5%**	**73.6%**	**78.8%**	**72.1%**	**89.2%**
Overall accuracy	**92.3%**	**92.8%**	**93.3%**	**94.1%**	**93.4%**	**92.6%**

5. Discussion

Our results show that shifting cultivation affected 32.9% ± 1.9% of Laos from 1991 to 2020 and the slash-and-burn activities increased significantly in the most recent 5-year period. From 1991 to 2005, the slash-and-burn activities increased gradually, and slightly decreased in 2006-2010 and remained the same until 2015. Recently, slash-and-burn activities increased from

12% of Laos in 2011-2015 to 15% in 2016-2020. Note that in this analysis, the area estimates include slash-and-burn activities that occurred in both previously and newly shifting cultivated fields.

In our map, most errors of *Shifting cultivation* were due to misclassification between *Stable forest* and *Shifting cultivation*. Commission of *Shifting cultivation* errors occurred mostly during dry conditions which cause a decrease in NDFI that may result in a break in CCDC-SMA model (**Fig. 22**). In this case, the break may be misclassified as *Shifting cultivation* if the minimum differences of NDFI during and before the break year exceeds the threshold. Although object-based analysis partly solves this problem, it is still difficult to separate *Drought* and *Shifting cultivation* in a highly fragmented and complex landscape – an example of such a situation is shown in **Fig. 22**. The omission errors of *Shifting cultivation* usually occurred at the edge of patches of *Shifting cultivation* or before 2000. 81% of the omission errors of *Shifting cultivation* occurred at the edge of *Shifting cultivation* (**Fig. 23** an example). This phenomenon of omission errors occurring at edges has been witnessed in other types of change studies as well, and methods have been proposed to mitigate the impact of such errors on area estimates (Olofsson et al., 2020). Because *Shifting cultivation* has such a large area weight and the reference sample was drawn by simple random sampling, such statistical technique was not necessary in this study. Another cause of omission errors was the relatively low data density before 2000. For example, in **Fig. 24**, although the slash-and-burn event in 1996 resulted in a large decrease in NDFI, no break was triggered as there was only one observation that significantly deviated from the predicted value of CCDC-SMA.

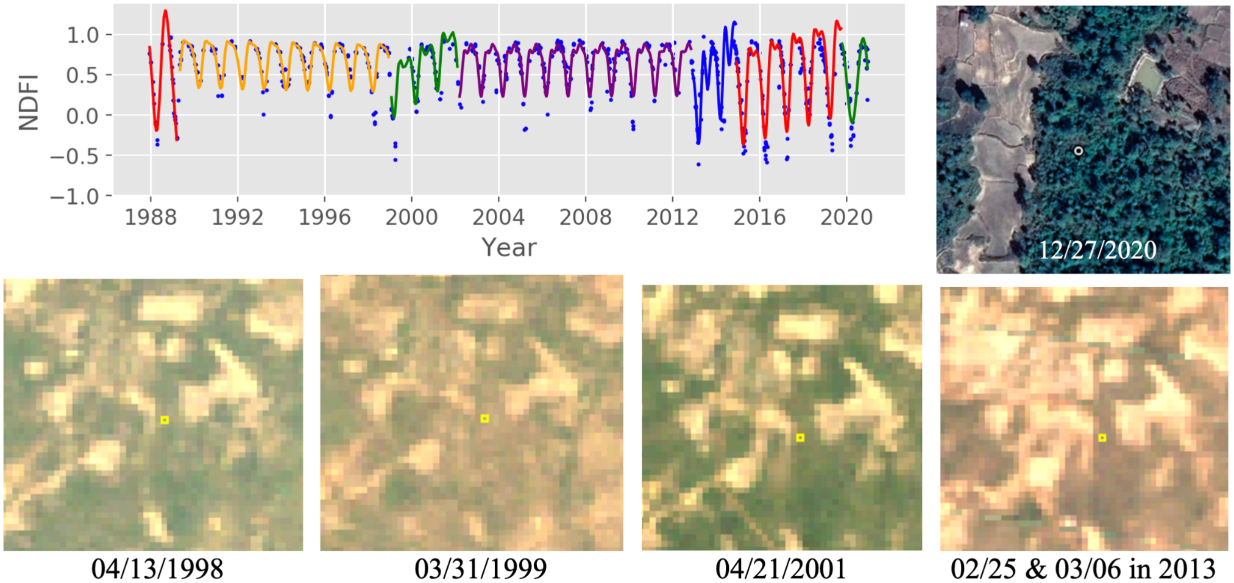

Fig. 22 An example of a commission error of *Shifting cultivation*. The disturbances in 1999 and 2013 were caused by drought but misclassified as *Shifting cultivation*. (Example location: 16°33'19"N, 104°58'15"E. In the time series plot, the blue points are Landsat observations, and the colored lines are the CCDC-SMA model fits, where different colors indicate different segments. In the Landsat images (Red-green-blue), the yellow squares show the pixel location. In the high-resolution images, the white circles show the center of the pixel.)

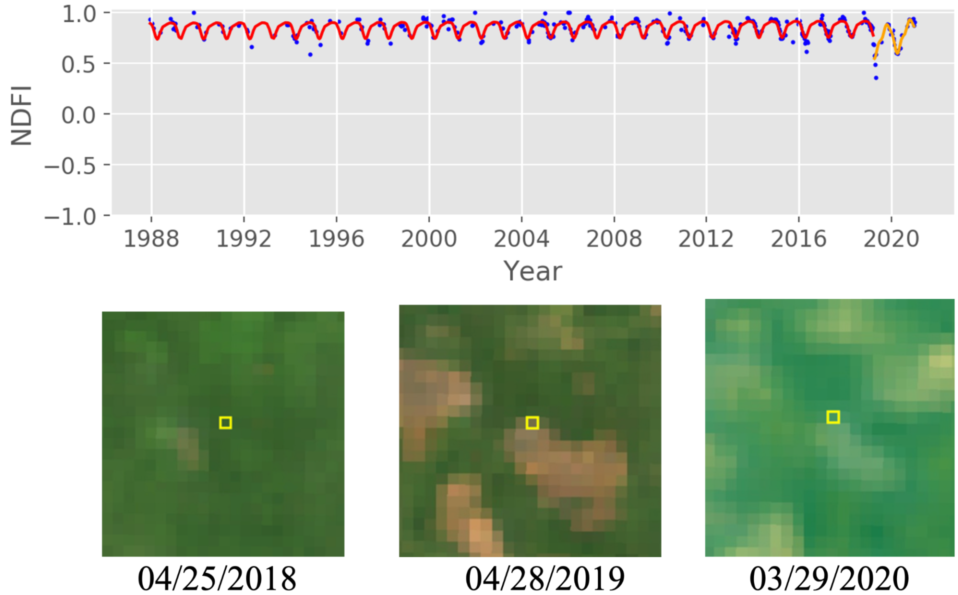

Fig. 23 An example of omission error of *Shifting cultivation*. The sample unit is located at the edge of a patch of shifting cultivation that occurred in 2019 but was misclassified as *Stable forest*. (Example location: 20°22'3"N, 100°25'46"E. In the time series plot, the blue points are Landsat observations, and the colored lines are the CCDC-SMA model fits, where different colors indicate different segments. In the Landsat images (Red-green-blue), the yellow squares show the pixel location.)

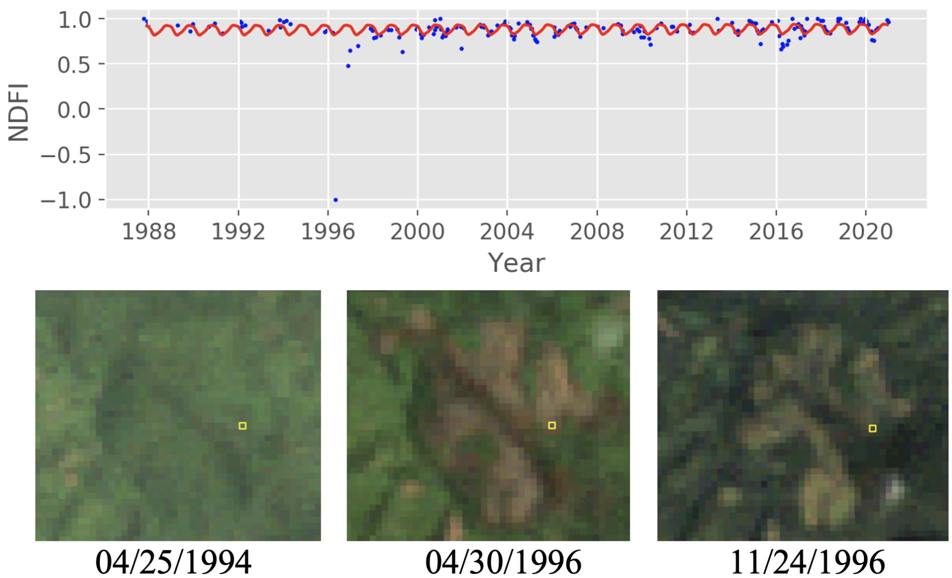

Fig. 24 An example of omission error due to low data density of Landsat in the early years. Shifting cultivation happened in 1996 but was misclassified as *Stable forest*. (Example location: 20° 3'1"N, 104° 3'16"E. In the time series plot, the blue points are Landsat observations, and the colored lines are the CCDC-SMA model fits, where different colors indicate different segments. In the Landsat images (Red-green-blue), the yellow squares show the pixel location.)

There are a few directions for our future research. First, we will analyze the spatial-temporal patterns of shifting cultivation based on our results and put the results in a socio-economic context. More analysis of the impact of change of fallow length and number of cycles of shifting cultivation is needed. Fallow length is an important characteristic of shifting cultivation and analysis of changes of fallow length is required for understanding the long-term impact of shifting cultivation. We will also investigate the geographic factors that influence the occurrence and frequency of shifting cultivation. Second, future research will quantify the carbon dynamics associated with shifting cultivation. The current guidelines for reporting of carbon dynamics associated with shifting cultivation in the REDD+ context are incomplete (GFOI, 2020). Shifting cultivation is a complicated process that involves highly dynamic carbon emissions and sequestration, which will require methods that go beyond those used for estimating emissions from deforestation. In the long term, the carbon emissions and sequestration of shifting cultivation depend on the fallow length and recovery status. In the future, we hope to combine our results on shifting cultivation with Global Ecosystem Dynamics Investigation (GEDI) data to investigate the effect of shifting cultivation on biomass. Third, the method to attribute forest disturbances can be expanded to a larger region, for example Southeast Asia. In the future, we will expand our research of attribution of forest disturbance to the whole of Southeast Asia.

6. Conclusion

We developed a method on GEE that combines CCDC-SMA, object-based analysis and post-disturbed land cover classification to monitor shifting cultivation. With the method, we were able to map 30 years of shifting cultivation across Laos with producer's accuracy of 88%, user's accuracy of 80% and the margin of error of area estimates of 6%. Our method is capable of detecting the highly-dynamic cycles of change associated with shifting cultivation, where traditional change detection methods are unable to accomplish. Our method and products are useful for estimating carbon emissions resulting from shifting cultivation, which are now rarely included in greenhouse gas inventories even if stipulated by international reporting guidelines. Furthermore, our research indicates that forest disturbance can be attributed at the pixel-level by combining time series analysis and object-based image analysis. We found that object-based image analysis is useful for separating large-scale natural disturbance from fine-scale anthropogenic disturbance. Finally, our products and results provide valuable information for policy makers in terms of understanding the extent and trends of shifting cultivation. Our results indicate that shifting cultivation accounts for 33% ± 2% of Laos and the slash-and-burn activities have increased in recent years, which policy makers should pay attention to.

7. Acknowledgements

This research was funded by the NASA Land-Cover and Land-Use Change Program (grant number: 80NSSC18K0315) (PI: Pontus Olofsson), the NASA Carbon Monitoring System (grant number: 80NSSC20K0022) (PI: Pontus Olofsson) and USGS Landsat Science Team Program for Better Use of the Landsat Temporal Domain: Monitoring Land Cover Type, Condition and Change (grant number: G12PC00070) (PI: Curtis Woodcock). We also greatly appreciate Kangjoon Cho and Hanfeng Gu for assisting with the sample interpretation.

References:

Abatzoglou, J.T., Dobrowski, S.Z., Parks, S.A., Hegewisch, K.C., 2018. TerraClimate, a high-resolution global dataset of monthly climate and climatic water balance from 1958-2015. Sci. Data 5, 1–12. https://doi.org/10.1038/sdata.2017.191

Adhikary, P.P., Barman, D., Madhu, M., Dash, C.J., Jakhar, P., Hombegowda, H.C., Naik, B.S., Sahoo, D.C., Beer, K., 2019. Land use and land cover dynamics with special emphasis on shifting cultivation in Eastern Ghats Highlands of India using remote sensing data and

GIS. Environ. Monit. Assess. 191. https://doi.org/10.1007/s10661-019-7447-7

Arévalo, P., Olofsson, P., Woodcock, C.E., 2019. Continuous monitoring of land change activities and post-disturbance dynamics from Landsat time series : A test methodology for REDD + reporting. Remote Sens. Environ. 1–14. https://doi.org/10.1016/j.rse.2019.01.013

Arévalo, P., Bullock, E.L., Woodcock, C.E., Olofsson, P., 2020. A Suite of Tools for Continuous Land Change Monitoring in Google Earth Engine. Front. Clim. 2, 1–19.

Belgiu, M., Csillik, O., 2018. Sentinel-2 cropland mapping using pixel-based and object-based time-weighted dynamic time warping analysis. Remote Sens. Environ. 204, 509–523. https://doi.org/10.1016/j.rse.2017.10.005

Bullock, E.L., Woodcock, C.E., Olofsson, P., 2020. Monitoring tropical forest degradation using spectral unmixing and Landsat time series analysis. Remote Sens. Environ. 238, 110968. https://doi.org/10.1016/j.rse.2018.11.011

Butler, J.H., 1980. Economic Geography: Spatial and Environmental Aspects of Economic Activity. John Wiley & Sons.

Carlson, T.N. and Ripley, D.A., 1997. On the relation between NDVI, fractional vegetation cover, and leaf area index. Remote sensing of Environment, 62(3), pp.241-252.

Chen, S., Woodcock, C.E., Bullock, E.L., Arévalo, P., Torchinava, P., Peng, S., Olofsson, P., 2021. Monitoring temperate forest degradation on Google Earth Engine using Landsat time series analysis. Remote Sens. Environ. 265, 112648. https://doi.org/10.1016/j.rse.2021.112648

Costa, H., Foody, G.M., Boyd, D.S., 2017. Using mixed objects in the training of object-based image classifications. Remote Sens. Environ. 190, 188–197.

https://doi.org/10.1016/j.rse.2016.12.017
Cramb, R., 2020. White gold: The commercialisation of rice farming in the lower Mekong Basin (p. 456). Springer Nature.
Curtis, P.G., Slay, C.M., Harris, N.L., Tyukavina, A., Hansen, M.C., 2018. Classifying drivers of global forest loss. Science (80-.). 361, 1108–1111. https://doi.org/10.1126/science.aau3445
Das, P., Mudi, S., Behera, M.D., Barik, S.K., Mishra, D.R., Roy, P.S., 2021. Automated mapping for long-term analysis of shifting cultivation in northeast India. Remote Sens. 13. https://doi.org/10.3390/rs13061066
Department of Forestry, Ministry of Agriculture and Forestry, Lao PDR, 2018. Lao PDR's Forest Reference Emission Level and Forest Reference Level for REDD+ Results Payment under the UNFCCC.
Dutrieux, L.P., Jakovac, C.C., Latifah, S.H., Kooistra, L., 2016. Reconstructing land use history from Landsat time-series: Case study of a swidden agriculture system in Brazil. Int. J. Appl. Earth Obs. Geoinf. 47, 112–124. https://doi.org/10.1016/j.jag.2015.11.018
Epprecht, M., Weber, A.K., Bernhard, R., Keoka, K., Saphangthong, T., Manivong, V., Ingxay, P., Vongsamphanh, P., Bosoni, N., Hanephom, S. and Vanmeexai, P., 2018. Atlas of agriculture in the Lao PDR: patterns and trends between 1999 & 2011. Centre for Development and Environment (CDE), University of Bern, Switzerland, and Ministry of Agriculture and Forestry (MAF), Lao PDR, with Bern Open Publishing (BOP). p70. https://www.k4d.la/publications/
FCPF, 2020. Guidelines on the application of the methodological framework Number 2 - On technical corrections to GHG emissions and removals reported in the reference period.

https://www.forestcarbonpartnership.org/sites/fcp/files/FCPF%20Guidelines%20on%20the%20Application%20of%20the%20Methodological%20Framework%20Number%202_2020_0.pdf

GFOI, 2020. Integration of remote-sensing and ground-based observations for estimation of emissions and removals of greenhouse gases in forests: Methods and Guidance from the Global Forest Observations Initiative, Edition 3.0, Food and Agriculture Organization, Rome.

Gorelick, N., Hancher, M., Dixon, M., Ilyushchenko, S., Thau, D., Moore, R., 2017. Google Earth Engine: Planetary-scale geospatial analysis for everyone. Remote Sens. Environ. 202, 18–27. https://doi.org/10.1016/j.rse.2017.06.031

Hansen, M.C., Potapov, P. V., Moore, R., Hancher, M., Turubanova, S.A.A., Tyukavina, A., ... & Kommareddy, A., 2013. High-Resolution Global Maps of 21st-Century Forest Cover Change. Science 342, 850–853. https://doi.org/10.1126/science.1244693

Heinimann, A., Hett, C., Hurni, K., Messerli, P., Epprecht, M., Jørgensen, L. and Breu, T., 2013. Socio-economic perspectives on shifting cultivation landscapes in Northern Laos. *Human Ecology*, *41*(1), pp.51-62.

Heinimann, A., Mertz, O., Frolking, S., Christensen, A.E., Hurni, K., Sedano, F., Chini, L.P., Sahajpal, R., Hansen, M., Hurtt, G., 2017. A global view of shifting cultivation: Recent, current, and future extent. PLoS One 12, 1–22. https://doi.org/10.1371/journal.pone.0184479

Hermosilla, T., Wulder, M.A., White, J.C., Coops, N.C., Hobart, G.W., 2015. Regional detection, characterization, and attribution of annual forest change from 1984 to 2012 using Landsat-derived time-series metrics. Remote Sens. Environ. 170, 121–132.

https://doi.org/10.1016/j.rse.2015.09.004

Herold, M., Skutsch, M., 2011. Monitoring, reporting and verification for national REDD + programmes: Two proposals. Environ. Res. Lett. 6. https://doi.org/10.1088/1748-9326/6/1/014002

Hett, C., Castella, J.C., Heinimann, A., Messerli, P., Pfund, J.L., 2012. A landscape mosaics approach for characterizing swidden systems from a REDD+ perspective. Appl. Geogr. 32, 608–618. https://doi.org/10.1016/j.apgeog.2011.07.011

Hillel, D., 2007. Soil in the environment: crucible of terrestrial life. Elsevier.

Hurni, K., Hett, C., Epprecht, M., Messerli, P., Heinimann, A., 2013a. A texture-based land cover classification for the delineation of a shifting cultivation landscape in the lao PDR using landscape metrics. Remote Sens. 5, 3377–3396. https://doi.org/10.3390/rs5073377

Hurni, K., Hett, C., Heinimann, A., Messerli, P., Wiesmann, U., 2013b. Dynamics of Shifting Cultivation Landscapes in Northern Lao PDR Between 2000 and 2009 Based on an Analysis of MODIS Time Series and Landsat Images. Hum. Ecol. 41, 21–36. https://doi.org/10.1007/s10745-012-9551-y

Kennedy, R.E., Yang, Z., Cohen, W.B., 2010. Detecting trends in forest disturbance and recovery using yearly Landsat time series: 1. LandTrendr - Temporal segmentation algorithms. Remote Sens. Environ. 114, 2897–2910. https://doi.org/10.1016/j.rse.2010.07.008

Kurien, A.J., Lele, S., Nagendra, H., 2019. Farms or Forests? Understanding and mapping shifting cultivation using the case study of West Garo hills, India. Land 8. https://doi.org/10.3390/land8090133

Jakovac, C.C., Dutrieux, L.P., Siti, L., Peña-Claros, M., Bongers, F., 2017. Spatial and temporal dynamics of shifting cultivation in the middle-Amazonas river: Expansion and intensification. PLoS One 12, 1–15. https://doi.org/10.1371/journal.pone.0181092

Jin, S. and Sader, S.A., 2005. Comparison of time series tasseled cap wetness and the normalized difference moisture index in detecting forest disturbances. Remote sensing of Environment, 94(3), pp.364-372.

Langner, A., Miettinen, J., Kukkonen, M., Vancutsem, C., Simonetti, D., Vieilledent, G., Verhegghen, A., Gallego, J., Stibig, H.J., 2018. Towards operational monitoring of forest canopy disturbance in evergreen rain forests: A test case in continental Southeast Asia. Remote Sens. 10, 1–21. https://doi.org/10.3390/rs10040544

Leisz, S.J., Rasmussen, M.S., 2012. Mapping fallow lands in Vietnam's north-central mountains using yearly Landsat imagery and a land-cover succession model. Int. J. Remote Sens. 33, 6281–6303. https://doi.org/10.1080/01431161.2012.681712

Li, P., Feng, Z., Jiang, L., Liao, C., Zhang, J., 2014. A review of swidden agriculture in Southeast Asia. Remote Sens. 6, 1654–1683. https://doi.org/10.3390/rs6021654

Li, P., Feng, Z., Xiao, C., Boudmyxay, K., Liu, Y., 2018. Detecting and mapping annual newly-burned plots (NBP) of swiddening using historical Landsat data in Montane Mainland Southeast Asia (MMSEA) during 1988–2016. J. Geogr. Sci. 28, 1307–1328. https://doi.org/10.1007/s11442-018-1527-4

Liao, C., Feng, Z., Li, P., Zhang, J., 2015. Monitoring the spatio-temporal dynamics of swidden agriculture and fallow vegetation recovery using Landsat imagery in northern Laos. J. Geogr. Sci. 25, 1218–1234. https://doi.org/10.1007/s11442-015-1229-0

Manivong, V. and Cramb, R., 2020. From Subsistence to Commercial Rice Production in Laos. In *White Gold: The Commercialisation of Rice Farming in the Lower Mekong Basin* (pp.

103-119). Palgrave Macmillan, Singapore. https://doi.org/10.1007/978-981-15-0998-8

Messerli, P., Heinimann, A., Epprecht, M., 2009. Finding homogeneity in heterogeneity - A new approach to quantifying landscape mosaics developed for the Lao PDR. Hum. Ecol. 37, 291–304. https://doi.org/10.1007/s10745-009-9238-1

Miettinen, J., Stibig, H.J., Achard, F., 2014. Remote sensing of forest degradation in Southeast Asia-Aiming for a regional view through 5-30 m satellite data. Glob. Ecol. Conserv. 2, 24–36. https://doi.org/10.1016/j.gecco.2014.07.007

Miller, J.D. and Thode, A.E., 2007. Quantifying burn severity in a heterogeneous landscape with a relative version of the delta Normalized Burn Ratio (dNBR). Remote Sensing of Environment, 109(1), pp.66-80.

Molinario, G., Hansen, M.C., Potapov, P. V., 2015. Forest cover dynamics of shifting cultivation in the Democratic Republic of Congo: A remote sensing-based assessment for 2000-2010. Environ. Res. Lett. 10. https://doi.org/10.1088/1748-9326/10/9/094009

Müller, D., Suess, S., Hoffmann, A.A., Buchholz, G., 2013. The Value of Satellite-Based Active Fire Data for Monitoring, Reporting and Verification of REDD+ in the Lao PDR. Hum. Ecol. 41, 7–20. https://doi.org/10.1007/s10745-013-9565-0

Olofsson, P., Arévalo, P., Espejo, A.B., Green, C., Lindquist, E., McRoberts, R.E., Sanz, M.J., 2020. Mitigating the effects of omission errors on area and area change estimates. Remote Sens. Environ. 236, 111492. https://doi.org/10.1016/j.rse.2019.111492

Olofsson, P., Foody, G.M., Herold, M., Stehman, S. V., Woodcock, C.E., Wulder, M.A., 2014. Good practices for estimating area and assessing accuracy of land change. Remote Sens. Environ. 148, 42–57. https://doi.org/10.1016/j.rse.2014.02.015

Olofsson, P., Foody, G.M., Stehman, S. V., Woodcock, C.E., 2013. Making better use of accuracy data in land change studies: Estimating accuracy and area and quantifying uncertainty using stratified estimation. Remote Sens. Environ. 129, 122–131. https://doi.org/10.1016/j.rse.2012.10.031

Palmer, W.C., 1965. Meteorological Drought. U.S. Weather Bureau, Washington, D.C. Research paper No. 45. https://www.ncdc.noaa.gov/temp-and-precip/drought/docs/palmer.pdf

Potapov, P., Tyukavina, A., Turubanova, S., Talero, Y., Hernandez-Serna, A., Hansen, M.C., Saah, D., Tenneson, K., Poortinga, A., Aekakkararungroj, A., Chishtie, F., Towashiraporn, P., Bhandari, B., Aung, K.S., Nguyen, Q.H., 2019. Annual continuous fields of woody vegetation structure in the Lower Mekong region from 2000-2017 Landsat time-series. Remote Sens. Environ. 232, 111278. https://doi.org/10.1016/j.rse.2019.111278

Rendenieks, Z., Nita, M.D., Nikodemus, O., Radeloff, V.C., 2020. Half a century of forest cover change along the Latvian-Russian border captured by object-based image analysis of Corona and Landsat TM/OLI data. Remote Sens. Environ. 249. https://doi.org/10.1016/j.rse.2020.112010

Roder, W., 2000. Slash-and-burn Rice Systems in the Hills of Northern Lao PDR. Int. Rice Res. Inst..

Roy, D.P., Boschetti, L. and Trigg, S.N., 2006. Remote sensing of fire severity: assessing the performance of the normalized burn ratio. IEEE Geoscience and Remote Sensing Letters, 3(1), pp.112-116.

Saah, D., Tenneson, K., Poortinga, A., Nguyen, Q., Chishtie, F., Aung, K.S., Markert, K.N...., Ganz, D., 2020. Primitives as building blocks for constructing land cover maps. Int. J. Appl. Earth Obs. Geoinf. 85, 101979. https://doi.org/10.1016/j.jag.2019.101979

Saphangthong, T. and Kono, Y., 2009. Continuity and discontinuity in land use changes: a case study in Northern Lao villages. Japanese Journal of Southeast Asian Studies, 47(3), pp.263-286. https://kyoto-seas.org/pdf/47/3/4703all.pdf

Silva, J.M.N., Carreiras, J.M.B., Rosa, I., Pereira, J.M.C., 2011. Greenhouse gas emissions from shifting cultivation in the tropics, including uncertainty and sensitivity analysis. J. Geophys. Res. Atmos. 116, 1–21. https://doi.org/10.1029/2011JD016056

Stehman, S. V., 2013. Estimating area from an accuracy assessment error matrix. Remote Sens. Environ. 132, 202–211. https://doi.org/10.1016/j.rse.2013.01.016

Tang, X., Woodcock, C.E., Olofsson, P., Hutyra, L.R., 2021. Spatiotemporal assessment of land use/land cover change and associated carbon emissions and uptake in the Mekong River Basin. Remote Sens. Environ. 256, 112336. https://doi.org/10.1016/j.rse.2021.112336

The Government of Lao PDR, Forestry Strategy to the year 2020 of the Lao PDR. 2020. https://forestlegality.org/sites/default/files/country_documents/Forestry%20Strategy%202020%20of%20the%20LAO%20PDR_0.pdf

Therien, C., 2018. PySptools. https://pysptools.sourceforge.io/

Toure, S.I., Stow, D.A., Shih, H. chien, Weeks, J., Lopez-Carr, D., 2018. Land cover and land use change analysis using multi-spatial resolution data and object-based image analysis. Remote Sens. Environ. 210, 259–268. https://doi.org/10.1016/j.rse.2018.03.023

Van Vliet, N., Mertz, O., Heinimann, A., Langanke, T., Pascual, U., Schmook, B., Adams, C., Schmidt-Vogt, D., Messerli, P., Leisz, S., Castella, J.C., Jørgensen, L., Birch-Thomsen, T., Hett, C., Bruun, T.B., Ickowitz, A., Vu, K.C., Yasuyuki, K., Fox, J., Padoch, C., Dressler, W., Ziegler, A.D., 2012. Trends, drivers and impacts of changes in swidden cultivation in tropical forest-agriculture frontiers: A global assessment. Glob. Environ.

Chang. 22, 418–429. https://doi.org/10.1016/j.gloenvcha.2011.10.009

Verbesselt, J., Hyndman, R., Newnham, G., Culvenor, D., 2010. Detecting trend and seasonal changes in satellite image time series. Remote Sens. Environ. 114, 106–115. https://doi.org/10.1016/j.rse.2009.08.014

Villa, P.M., Rodrigues, A.C., Martins, S.V., de Oliveira Neto, S.N., Laverde, A.G., Riera-Seijas, A., 2021. Reducing intensification by shifting cultivation through sustainable climate-smart practices in tropical forests: A review in the context of UN Decade on Ecosystem Restoration. Curr. Res. Environ. Sustain. 3, 100058. https://doi.org/10.1016/j.crsust.2021.100058

Von Grebmer, K., Bernstein, J., Mukerji, R., Patterson, F., Wiemers, M., Ní Chéilleachair, R., Foley, C., Gitter, S., Ekstrom, K., Fritschel, H., 2019. 2019 Global Hunger Index: The Challenge of Hunger and Climate Change. The International Food Policy Research Institute (IFPRI). Dublin and Bonn. https://www.globalhungerindex.org/pdf/en/2019.pdf

Wells, N., Goddard, S., Hayes, M.J., 2004. A self-calibrating Palmer Drought Severity Index. J. Clim. 17, 2335–2351. https://journals.ametsoc.org/view/journals/clim/17/12/1520-0442_2004_017_2335_aspdsi_2.0.co_2.xml

Wiesmann, D., 2006. A global hunger index: Measurement concept, ranking of countries, and trends (Vol. 212). Intl Food Policy Res Inst.

Winter, M.E., 1999. N-FINDR: An algorithm for fast autonomous spectral end-member determination in hyperspectral data. Imaging Spectrometry V. International Society for Optics and Photonics. Vol. 3753, pp. 266-275. https://doi.org/10.1117/12.366289

Woodcock, C.E., Allen, R.G., Anderson, M., Belward, A., Bindschadler, R., Cohen, W.B., ... Wynne, R., 2008. Free access to Landsat imagery. Science 320 (5879), 1011.

Woodcock, C.E., Loveland, T.R., Herold, M., Bauer, M.E., 2020. Transitioning from change detection to monitoring with remote sensing: A paradigm shift. Remote Sens. Environ. 238, 111558. https://doi.org/10.1016/j.rse.2019.111558

Yu, W., Zhou, W., Qian, Y., Yan, J., 2016. A new approach for land cover classification and change analysis: Integrating backdating and an object-based method. Remote Sens. Environ. 177, 37–47. https://doi.org/10.1016/j.rse.2016.02.030

Ziegler, A.D., Phelps, J., Yuen, J.Q., Webb, E.L., Lawrence, D., Fox, J.M., Bruun, T.B., Leisz, S.J., Ryan, C.M., Dressler, W., Mertz, O., Pascual, U., Padoch, C., Koh, L.P., 2012. Carbon outcomes of major land-cover transitions in SE Asia: Great uncertainties and REDD+ policy implications. Glob. Chang. Biol. 18, 3087–3099. https://doi.org/10.1111/j.1365-2486.2012.02747.x

Zhu, Z., Woodcock, C.E., 2014. Continuous change detection and classification of land cover using all available Landsat data. Remote Sens. Environ. 144, 152–171. https://doi.org/10.1016/j.rse.2014.01.011

List of Figures

Fig. 3 Spectral reflectance of the endmembers.

Fig. 4 RMSE of SMA model of dry season in 2020. (The reflectance is scaled by 10,000.)

Fig. 5 Optimal threshold for the change magnitude used to classify breaks into *Forest disturbance* and *Undisturbed forest*. The plots show the accuracies and errors of these tests. (Max_Accuracy: maximum overall accuracy; Opt_Threshold: Optimal threshold; T: Thresholds)

Fig. 6 Time series of an example of shifting cultivation. Slash-and-burn events occurred in 2001, 2006, 2010, and 2017. The Landsat images captured the events and the fallow periods. The three Landsat images in 2017 captured the "slash-and-burn" process: The images on 03/21 and 04/06 show the "slash" process and the image on 05/08 shows the "burn" process. (Example location: 20° 2' 14"N, 100° 50' 7" E. In the time series plot, the blue points are the Landsat observations, and the colored lines are the CCDC-SMA model fits, where different colors indicate different segments. In the Landsat images (Red-green-blue), the yellow squares show the pixel location.)

Fig. 7 Time series of an example that includes both shifting cultivation and a rubber plantation. Clearing for shifting cultivation occurred in 1991 and 2001. In 2006, the land was cleared for rubber plantation. The Landsat images show the stages of shifting cultivation and the high-resolution images show the plantation. (Example location: 20°27'35"N, 101°24'50"E. In the time series plot, the blue points are Landsat observations, and the colored lines are the CCDC-SMA model fits, where different colors indicate different segments. In the Landsat images (Red-green-blue), the yellow squares show the pixel location. In the high-resolution images, the white circles show the center of the pixel.)

Fig. 8 Time series of an example of deforestation that occurred in 2011. Both the Landsat images and the high-resolution images show that the land cover was permanently converted from forest to non-forest. (Example location: 17°56'10"N, 102°40'45"E. In the time series plot, the blue points are Landsat observations, and the colored lines are the CCDC-SMA model fits, where different colors indicate different segments. In the Landsat images (Red-green-blue), the yellow squares show the pixel location.)

Fig. 9 Time series of an example of severe drought in 2016. The three Landsat images were acquired before, during and after the disturbance. (Example location: 20°17'8"N, 103°18'25"E. In the time series plot, the blue points are Landsat observations, and the colored lines are the CCDC-SMA model fits, where different colors indicate different segments. In the Landsat composites (Red-green-blue), the yellow points show the pixel location. The reddish-brown region was affected by severe drought.)

Fig. 10 Time series of an example of subtle disturbance. Selective logging occurred in November 1994, and a mild drought affected this location in 2016. (Example location: 20°17'40"N, 103°10'30"E. In the time series plot, the blue points are Landsat observations, and the colored lines are the CCDC-SMA model fits, where different colors indicate different segments. In the Landsat images (Red-green-blue), the yellow squares show the pixel location.)

Fig. 11 Land cover map of Laos in 2020 as an example of the annual land cover maps of 1990 - 2020.

Fig. 12 Annual Palmer Drought Severity Index (PDSI) for Laos calculated from the TerraClimate data (Abatzoglou et al., 2018).

Fig. 13 (a): Size of objects identified as *Forest disturbance*; (b): Histogram of the size of objects of *Drought* and *Shifting cultivation*.

Fig. 14 Optimal threshold of disturbance magnitude to differentiate *Shifting cultivation* and *Subtle disturbance*. The plots show the accuracies and errors of testing different thresholds. (Max_Accuracy: maximum overall accuracy of the tests; Opt_Threshold: Optimal threshold; T: Thresholds)

Fig. 15 Reference data collection. This sample unit was interpreted as "*Shifting cultivation*". The number of slash-and-burn events is 4, and the year of events are 1992, 2000, 2009, and 2018. (Sample unit location: 20°35'54"N, 101° 0'11"E. The images on the left side are Landsat images and a high-resolution image on Google Earth. The plots on the right side are Landsat observations of fraction of NPV, fraction of GV and NDFI. All these time series show significant change in each slash-and-burn event.)

Fig. 16 Disturbance map of Laos in 2016 as an example of annual disturbance maps from 1991-2020.

Fig. 17 First year of shifting cultivation in Laos. Places without shifting cultivation were mapped as *Stable forest, Permanent agriculture* and *Others*. In the magnified view of a region, shifting cultivation expanded from places adjacent to permanent agriculture to places close to stable forest.

Fig. 18 Annual area proportion of different disturbance types calculated from the map. The histograms are stacked, meaning that the total height of the bar for each year is the sum of the area proportions of all five types of disturbance for this year.

Fig. 19 Map of *Stable forest*, *Non-forest*, *Shifting cultivation*, *Deforestation* and *New plantation* of Laos during 1991-2020.

Fig. 20 Sampling-based area estimation (expressed in proportion) of *Stable forest*, *Non-forest*, *Shifting cultivation*, *Deforestation* and *New plantation* of Laos during 1991-2020. (Colored bars and numbers in red: The area estimates in proportion; black bar: error bar showing uncertainty of the estimates; blue cross: mapped area).

Fig. 21 Area estimates of slash and burn events by period during 1991-2020. (Colored bars and numbers in red: The area estimates in proportion; black bar: error bar showing uncertainty of the estimates; blue cross: mapped area)

Fig. 22 An example of a commission error of *Shifting cultivation*. The disturbances in 1999 and 2013 were caused by drought but misclassified as *Shifting cultivation*. (Example location: 16°33'19"N, 104°58'15"E. In the time series plot, the blue points are Landsat observations, and the colored lines are the CCDC-SMA model fits, where different colors indicate different segments. In the Landsat images (Red-green-blue), the yellow squares show the pixel location. In the high-resolution images, the white circles show the center of the pixel.)

Fig. 23 An example of omission error of *Shifting cultivation*. The sample unit is located at the edge of a patch of shifting cultivation that occurred in 2019 but was misclassified as *Stable forest*. (Example location: 20°22'3"N, 100°25'46"E. In the time series plot, the blue points are Landsat observations, and the colored lines are the CCDC-SMA model fits, where different colors indicate different segments. In the Landsat images (Red-green-blue), the yellow squares show the pixel location.)

Fig. 24 An example of omission error due to low data density of Landsat in the early years. Shifting cultivation happened in 1996 but was misclassified as *Stable forest*. (Example location: 20° 3'1"N, 104° 3'16"E. In the time series plot, the blue points are Landsat observations, and the colored lines are the CCDC-SMA model fits, where different colors indicate different segments. In the Landsat images (Red-green-blue), the yellow squares show the pixel location.)

List of Tables

Table 1 Surface reflectance of the endmembers collected in Laos (NIR: Near-infrared; SWIR: Short-wave infrared. The reflectance is scaled by 10,000).

Table 2 The mean of RMSE of the SMA model of seven selected years. (Scaled by 10,000.)

Table 3 Confusion matrix expressed in sample counts, mapped area and mapped area proportions of the classes.

Table 4 Sampling-based area estimates, accuracies and uncertainties of the classes.

Table 5 Sampling-based area estimates, accuracies and uncertainties of slash and burn events for the 5-year periods during 1991-2020.